



RESEARCH ARTICLE

10.1029/2022MS003331

Key Points:

- Cloud resolving model simulations capture robust aspects of mesoscale isotopic variations observed in tropical cyclones and squall lines
- Rain evaporation and rain-vapor diffusive exchanges are the main drivers of isotopic depletion within tropical cyclones and squall lines
- Horizontal advection spreads isotopic anomalies, thus reshaping the stable isotope patterns at the mesoscale

Supporting Information:

Supporting Information may be found in the online version of this article.

Correspondence to:

C. Risi,
Camille.Risi@lmd.ipsl.fr

Citation:

Risi, C., Muller, C., Vimeux, F., Blossey, P., Védeau, G., Dufaux, C., & Abramian, S. (2023). What controls the mesoscale variations in water isotopic composition within tropical cyclones and squall lines? Cloud resolving model simulations in radiative-convective equilibrium. *Journal of Advances in Modeling Earth Systems*, 15, e2022MS003331. <https://doi.org/10.1029/2022MS003331>

Received 1 AUG 2022
Accepted 20 MAR 2023

What Controls the Mesoscale Variations in Water Isotopic Composition Within Tropical Cyclones and Squall Lines? Cloud Resolving Model Simulations in Radiative-Convective Equilibrium

Camille Risi¹ , Caroline Muller¹, Françoise Vimeux^{2,3}, Peter Blossey⁴ , Grégoire Védeau^{1,3}, Clarisse Dufaux¹, and Sophie Abramian¹ 

¹Laboratoire de Météorologie Dynamique, IPSL, CNRS, École Normale Supérieure, Sorbonne Université, PSL Research University, Paris, France, ²HydroSciences Montpellier, Université de Montpellier, CNRS, IMT, IRD, Montpellier, France, ³Laboratoire des Sciences du Climat et de l'Environnement (CEA, CNRS, UVSQ), IPSL, Université Paris Saclay, Gif-sur-Yvette, France, ⁴Department of Atmospheric Sciences, University of Washington, Seattle, WA, USA

Abstract Water isotopes are tracers of convective processes and are often used as proxies for past precipitation. These applications require a better understanding of the impact of convective processes on the isotopic composition of water vapor and precipitation. One way to advance this understanding is to analyze the isotopic mesoscale variations during organized convective systems such as tropical cyclones or squall lines. The goal of this study is to understand these isotopic mesoscale variations with particular attention to isotopic signals in near-surface vapor and precipitation that may be present in observations and in paleoclimate proxies. With this aim, we run cloud resolving model simulations in radiative-convective equilibrium in which rotation or wind shear is added, allowing us to simulate tropical cyclones or squall lines. The simulations capture the robust aspects of mesoscale isotopic variations in observed tropical cyclones and squall lines. We interpret these variations using a simple water budget model for the sub-cloud layer of different parts of the domain. We find that rain evaporation and rain-vapor diffusive exchanges are the main drivers of isotopic depletion within tropical cyclones and squall lines. Horizontal advection spreads isotopic anomalies, thus reshaping the mesoscale isotopic pattern. This study contributes to our understanding of mesoscale isotopic variability and provides physical arguments supporting the interpretation of paleoclimate isotopic archives in tropical regions in terms of past cyclonic activity.

Plain Language Summary Naturally available, stable water molecules can be light (one oxygen atom and two hydrogen atoms) or heavy (one hydrogen atom is replaced by a deuterium atom). These different molecules are called water isotopes. In large, long-lived, severe storms such as tropical cyclones or squall lines (thunderstorms that organize into lines), the rain is observed to be more depleted in heavy isotopes. Several studies have exploited this property to reconstruct the past variations in the frequency of occurrence of tropical cyclones or severe thunderstorms based on isotope variations observed in speleothems. The aim of this study is to understand what controls the depletion in heavy isotopes of the rain in tropical cyclones and squall lines. With this aim, for the first time we use high-resolution simulations (2–4 km in horizontal) to simulate the internal dynamics of tropical cyclones and squall lines and their isotope composition. We design a simple model to interpret the results. We show that the rain evaporation and rain-vapor exchanges deplete the water vapor, and the subsequent rainfall, in heavy isotopes.

1. Introduction

The isotopic composition of water vapor (HDO or H_2^{18}O) evolves along the water cycle as phase changes are associated with isotopic fractionation. The isotopic composition of precipitation recorded in paleoclimate archives has significantly contributed to the reconstruction of past hydrological changes across the tropics (Cruz et al., 2009; Wang et al., 2001). Indeed, over tropical oceans, the precipitation is usually more depleted in heavy isotopes as precipitation rate increases, an observation called the amount effect (Dansgaard, 1964). In concert with the precipitation, the water vapor over tropical oceans is also more depleted as precipitation rate increases according to satellite and in situ observations (Kurita, 2013; Worden et al., 2007). Over tropical land, both the precipitation

and water vapor are generally observed to be more depleted as the precipitation rate increases on average over the previous days before the observation of isotopic depletion and on average over some large-scale domain upstream of the region of depletion, for example, in Western Africa (Risi et al., 2008; Tremoy et al., 2012), Southeast Tibetan Plateau (Gao et al., 2013), Southern India (Lekshmy et al., 2014; Sinha & Chakraborty, 2020), Southern tropical America (Vimeux et al., 2005, 2011) or the Maritime Continent (Conroy et al., 2016; Moerman et al., 2013). In the tropics, the importance of precipitation rate, either at the local or at the regional scale, in controlling the water isotopic composition of water vapor and precipitation is thus well established. However, the relationship between the water isotopic composition and precipitation rate can vary temporally and spatially. For example, it may depend on the proportion of stratiform versus convective rain (Aggarwal et al., 2016), on the organization of convection (Chakraborty et al., 2016; Lawrence et al., 2004; Risi et al., 2008) or on the shape of vertical velocity profiles (Lacour et al., 2017; Moore et al., 2014; Torri et al., 2017). For a more robust and quantitative interpretation of water isotopic archives in terms of past hydrological changes or cyclonic activity, a better understanding of how the precipitation rate impacts the isotopic composition of water vapor and precipitation is thus necessary.

In the tropics, most of the precipitation falls under deep convective systems (Houze, 2004). It is associated with processes which deplete the water vapor in heavy isotopes. In particular, observational studies have highlighted the role of rain evaporation (Worden et al., 2007), diffusive liquid-vapor exchanges (Lawrence et al., 2004), mesoscale downdrafts (Kurita, 2013; Risi et al., 2010) and microphysical processes in stratiform regions of convective systems (Aggarwal et al., 2016). Modeling studies with high resolution simulations have confirmed the key role of rain evaporation and diffusive liquid-vapor (Torri, 2021, 2022), and of microphysical processes in stratiform regions of convective systems, especially melting of depleted snow that subsequently evaporates (Risi et al., 2021).

One way to test the importance of these processes is to investigate the observed evolution of the isotopic composition of precipitation or near-surface water vapor within “organized” convective systems (Risi et al., 2010). By organized, we mean that the convective system has different parts, characterized by different convective or microphysical processes, and connected through some mesoscale circulation. For example, tropical cyclones are a spectacular manifestation of convective organization, usually with an eye at the center, surrounded by convective walls with intense rainfall and spiral rain bands reaching several hundreds of kilometers (Houze, 2010) (Figure 1a). The precipitation and near-surface water vapor collected in the vicinity of tropical cyclones often show stronger depletion toward the cyclone center, more depleted water vapor in spiral bands than in between bands (Bhattacharya et al., 2022; Gedzelman et al., 2003; Xu et al., 2019), and more enriched water vapor in the eye (Fudeyasu et al., 2008). The depletion has been interpreted in terms of progressive rain out toward the center and rain-vapor diffusive exchanges (Lawrence et al., 2002). The enrichment in the eye has been interpreted in terms of sea spray evaporation (Fudeyasu et al., 2008). As another example, squall lines are elongated, propagative convective systems with a gust front, followed by a convective region of intense rainfall, a transition region with a paused rainfall, and a trailing stratiform region of light rainfall (Houze, 2004) (Figure 1b). The precipitation collected during squall lines often features a W shape with more depleted rain in convective and stratiform regions (Risi et al., 2010; Taupin & Gallaire, 1998). In the near-surface water vapor, many squall lines show isotopic depletion in the convective and stratiform regions (Tremoy et al., 2014). This pattern has been interpreted in terms of rain evaporation and mesoscale downdrafts.

Better understanding the evolution of the isotopic composition of precipitation or near-surface water vapor within “organized” convective systems is also useful to better understand how convective organization is recorded in paleoclimate archives. In particular, more organized convective systems, such as squall lines (Maupin et al., 2021; Risi et al., 2008; Tremoy et al., 2014) or tropical cyclones (Chakraborty et al., 2016; Jackisch et al., 2022; Lawrence & Gedzelman, 1996; Lawrence et al., 2004; Price et al., 2008), have been observed to be associated with water vapor and precipitation that are more depleted in heavy isotopes than unorganized systems. In particular, the depleted rain of tropical cyclones leaves a depleted imprint in surface waters (Welsh & Sánchez-Murillo, 2020) and can significantly affect long-term averages of the isotopic composition of precipitation or surface waters (Baldini et al., 2016; Lawrence, 1998). This suggests that the annual-mean or multi-annual-mean isotopic composition of precipitation recorded in speleothems could be used to reconstruct past cyclonic activity (Chen et al., 2021; Frappier et al., 2007; Lawrence & Gedzelman, 2003; Miller et al., 2006), though this can be challenging (Jackisch et al., 2022). In the past few years, several studies have interpreted speleothems in terms of cyclonic frequency (Baldini et al., 2016; Medina-Elizalde & Rohling, 2012; Nott et al., 2007). Similarly, the depletion observed in Texan speleothems has been interpreted as enhanced activity of large, long-lived, organized convective systems

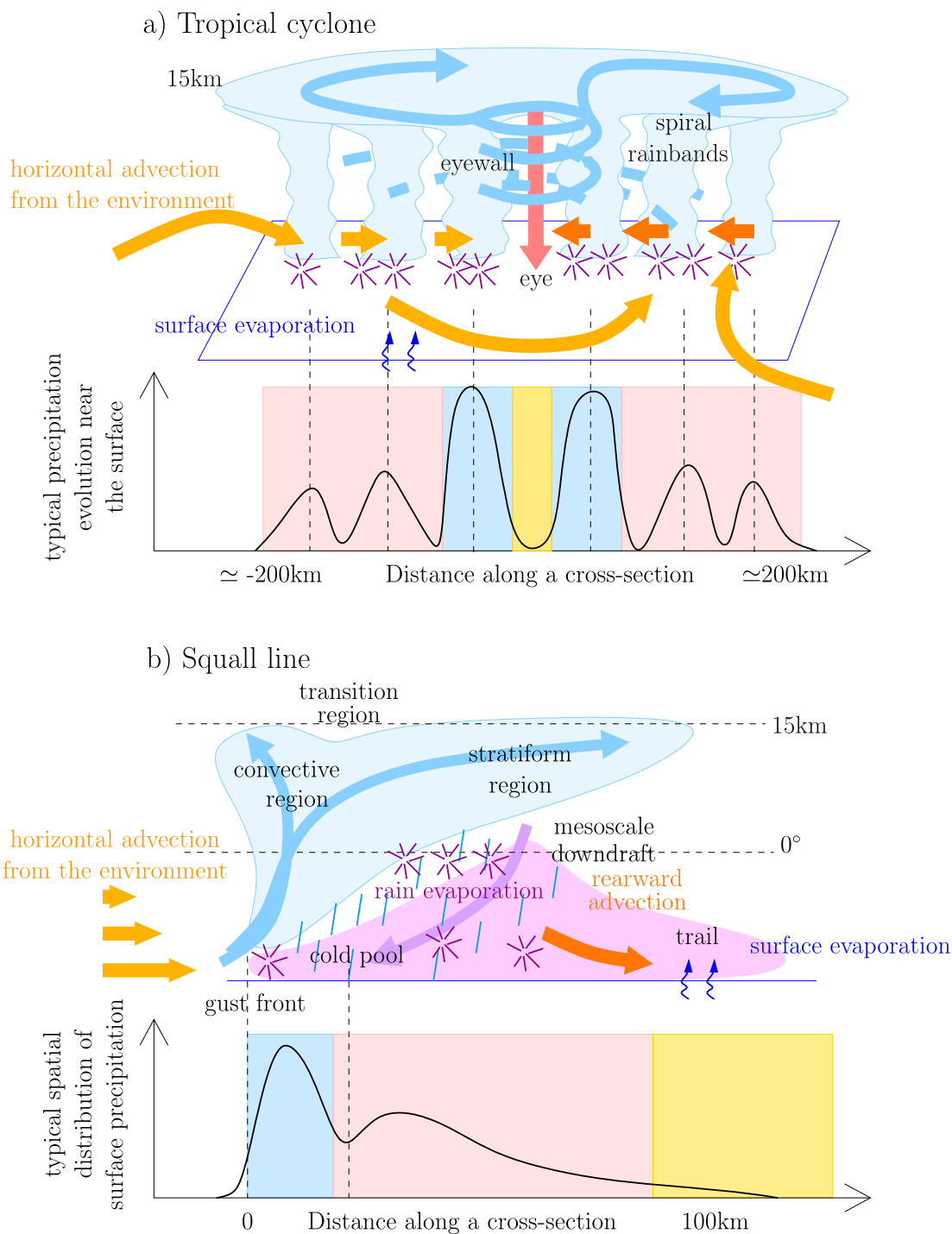


Figure 1. A schematic of the main structural elements of (a) tropical cyclones and (b) squall lines. The observed typical spatial distribution of the surface precipitation is also indicated. The vertical and horizontal scales are approximate and may vary depending on events. The yellow, blue, and pink rectangles in panel (a) respectively represent the eye, eyewall, and rain band regions of the cyclone, as will be defined later in the article; the blue, pink, and yellow rectangles in panel (b) respectively represent the convective, stratiform, and trail regions of the squall line, as will also be defined later in the article.

(Maupin et al., 2021). In addition to paleoclimate applications, better understanding how convective processes impact the water isotopic composition is also relevant to assess the added value of water isotopic measurements to better quantify convective processes and better evaluate their representation in models (Bony et al., 2008; Diekmann et al., 2021; Field et al., 2014; Ramos et al., 2022).

The goal of this paper is to investigate the processes controlling the evolution of near-surface water vapor and precipitation within squall lines and tropical cyclones. So far, this question has often been addressed using observational studies or simple box models (Bhattacharya et al., 2022; Fudeyasu et al., 2008; Gedzelman et al., 2003; Lawrence et al., 2002; Tremoy et al., 2014; Xu et al., 2019). Here for the first time, we used three-dimensional high-resolution simulations, in which convective motions are explicitly represented, to simulate the isotopic composition of water vapor and precipitation in tropical cyclones and squall lines. Using these simulations and a simple box model of the sub-cloud layer (SCL), we quantified the relative importance of the different processes that have been suggested by previous studies, for example, progressive rain out, rain-vapor exchange, downdrafts (Bhattacharya et al., 2022; Lawrence et al., 2002; Risi et al., 2010; Tremoy et al., 2014; Xu et al., 2019). Our simulations are run in a radiative-convective equilibrium configuration. Because of this idealized configuration, no one-to-one comparison can be made with real observed system. Therefore, we focus on robust features that have been observed in most squall lines and tropical cyclones in previous studies.

2. Methods

2.1. Isotopic Variables

The water content in heavy isotopes (HDO or $H_2^{18}O$) is expressed in ‰ as $\delta D = (R_D/R_{D,SMOW} - 1) \times 1000$ and $\delta^{18}O = (R_{18O}/R_{18O,SMOW} - 1) \times 1000$, where R_D and R_{18O} respectively are the ratio of Deuterium over Hydrogen atoms and of ^{18}O over ^{16}O atoms in the water, and SMOW is the Standard Mean Ocean Water reference. Hereafter, when there is a relatively large ratio of heavy over light atoms in some water, we will refer to this water as relatively enriched in heavy atoms, or simply relatively enriched. Conversely, when there is a relatively small ratio of heavy over light atoms in some water, we will refer to this water as relatively depleted in heavy atoms, or simply relatively depleted.

To first order, δD variations are 8 times those in $\delta^{18}O$ (Craig, 1961), so we will focus on δD here. However, slight deviations in the $\delta D - \delta^{18}O$ relationship can be quantified by the second-order parameter d-excess: $d = \delta D - 8 \cdot \delta^{18}O$. It reflects kinetic effects associated with diffusivity differences between the different water isotopologues. We will also show some results for d-excess as it can reflect kinetic effects in rain evaporation or surface evaporation.

2.2. Model and Simulations

2.2.1. Cloud Resolving Model

We used the same Cloud Resolving Model (CRM) as that used in Risi et al. (2020), namely the System for Atmospheric Modeling (SAM) non-hydrostatic model (Khairoutdinov & Randall, 2003), version 6.10.9, which is enabled with water isotopes (Blossey et al., 2010). This model solves anelastic conservation equations for momentum, mass, energy, and water, which is present in the model under six phases: water vapor, cloud liquid, cloud ice, precipitating liquid, precipitating snow, and precipitating graupel. We used the bulk, mixed-phase microphysical parameterization from (Thompson et al., 2008) in which water isotopes were implemented (Moore et al., 2016). At the ocean surface, there is no representation of sea spray. Therefore, we did not simulate the possible impact of sea spray on the isotopic composition in the eye (Fudeyasu et al., 2008).

2.2.2. Radiative-Convective Equilibrium With Large-Scale Forcing

Simulations are three-dimensional, with a doubly periodic domain. They are run in radiative-convective equilibrium over an ocean surface. The sea surface temperature (SST) was set at 30°C. We did not prescribe any diurnal cycle.

Organized convection is typically observed in regions of large-scale ascent (Jakob et al., 2019; Tan et al., 2013). Therefore, we impose a large-scale vertical ascent with a cubic shape, reaching -40 hPa/d at 5 km and 0 hPa/d at the surface and above 100 hPa (Risi et al., 2020). Simulations were also run without vertical ascent, and gave similar results except that the convective systems were smaller and with a less well-defined internal structure. For example, the tropical cyclone without ascent does not show any eye at the center. We thus focus on the simulations with large-scale ascent in the following.

The simulations were run for 50 days. The last 10 days of simulation are analyzed with one three-dimensional output file every day. In radiative-convective equilibrium, all snapshots exhibit similar behavior (Movies S1 and S2).

2.2.3. Set-Up for the Cyclone Simulation

We used a domain of $1,024 \times 1,024$ km with a horizontal resolution of 4 km and 96 vertical levels. This horizontal resolution is sufficient to properly simulate the internal structure of a cyclone (Gentry & Lackmann, 2010). Cyclones spontaneously develop in radiative-convective equilibrium simulations when some rotation is added (Khairoutdinov & Emanuel, 2013; Muller & Romps, 2018). Here the effect of rotation is added through a Coriolis parameter that corresponds to a latitude of 40° . Although no tropical cyclones are expected to form at such latitudes, a strong rotation allows us to simulate a small cyclone (Chavas & Emanuel, 2014) that can fit our small domain. This allows the simulation to remain computationally reasonable.

The initial conditions are spatially homogeneous and an unique cyclone develops spontaneously through self-aggregation mechanisms after a few days. This is consistent with the time scale for cyclogenesis in other self-aggregation studies (Muller & Romps, 2018).

2.2.4. Set-Up for the Squall Line Simulation

We used a domain of 256×256 km with a horizontal resolution of 2 km and 96 vertical levels. Squall lines spontaneously develop in radiative-convective equilibrium simulations when horizontal wind shear is added (Abramian et al., 2022; Muller, 2013; Robe & Emanuel, 2001). We added a horizontally uniform wind in the x direction that reaches 10 m/s at the surface and linearly decrease to 0 m/s at 1 km. According to Rotunno et al. (1988), the shear with our settings leads to the formation of a strong and long-lived squall line, perpendicular to the background wind. The uniform surface wind is subtracted when calculating surface fluxes, to avoid this simulation from having significantly higher surface fluxes. The radiative fluxes are imposed, because interactive radiation leads to some radiative feedbacks that disfavors the organization into squall lines. The convection quickly organizes into a line, after about 1 day of simulation.

2.3. Simple Box Model of the Sub-Cloud Layer

To quantify the relative importance of processes in determining the isotopic composition in the different parts of the domain, we design a simple box model for the SCL (Figure 2a). The model is the same as that in Risi et al. (2020), except that here we account for horizontal advection and non-stationary effects. Accounting for these effects is necessary because the simple model will be applied in the different sub-domains highlighted in Figure 1. Whereas the SCL is in quasi-equilibrium in the domain-mean, the SCL is not in quasi-equilibrium in sub-domains. For example, the eye of the cyclone wanders across the domain and is thus never in quasi-equilibrium.

Previous studies have used model tendencies along backward trajectories to quantify the relative importance of processes on local conditions (Attinger et al., 2019; Dütsch et al., 2018). This approach is most relevant when large-scale horizontal transport plays a key role. In radiative-convective equilibrium however, local processes and vertical transport dominate. A simple box model was thus judged more relevant.

2.3.1. Water Vapor Budget

The SCL is defined as the atmospheric levels from the surface to the SCL top, where the SCL top is the level just below the lowest level where the domain-mean massic cloud water content exceeds 10% of its maximum value. With this definition, we find that the SCL is approximately well-mixed in our simulations. Therefore, in the box model, we can assume that the specific humidity is vertically uniform throughout the SCL, consistent with previous mixed-layer models (Albright et al., 2022; Neggers et al., 2006; Stevens, 2006). We define W as the water mass in the SCL per area unit (in kg m^{-2}):

$$W = \int_{z=0}^{z_t} \rho \cdot q \cdot dz \quad (1)$$

where q is the specific humidity near the surface, ρ is the air density, z is the altitude above sea level, and z_t is the altitude of the SCL top. The water budget of the SCL in a given sub-domain writes (Figure 2a):

$$\frac{dW}{dt} = E_{sfc} + F_d \cdot q \cdot (r_d - 1) - F_u \cdot q \cdot (r_u - 1) + E_{horiz} + E_{cv} - E_c \quad (2)$$

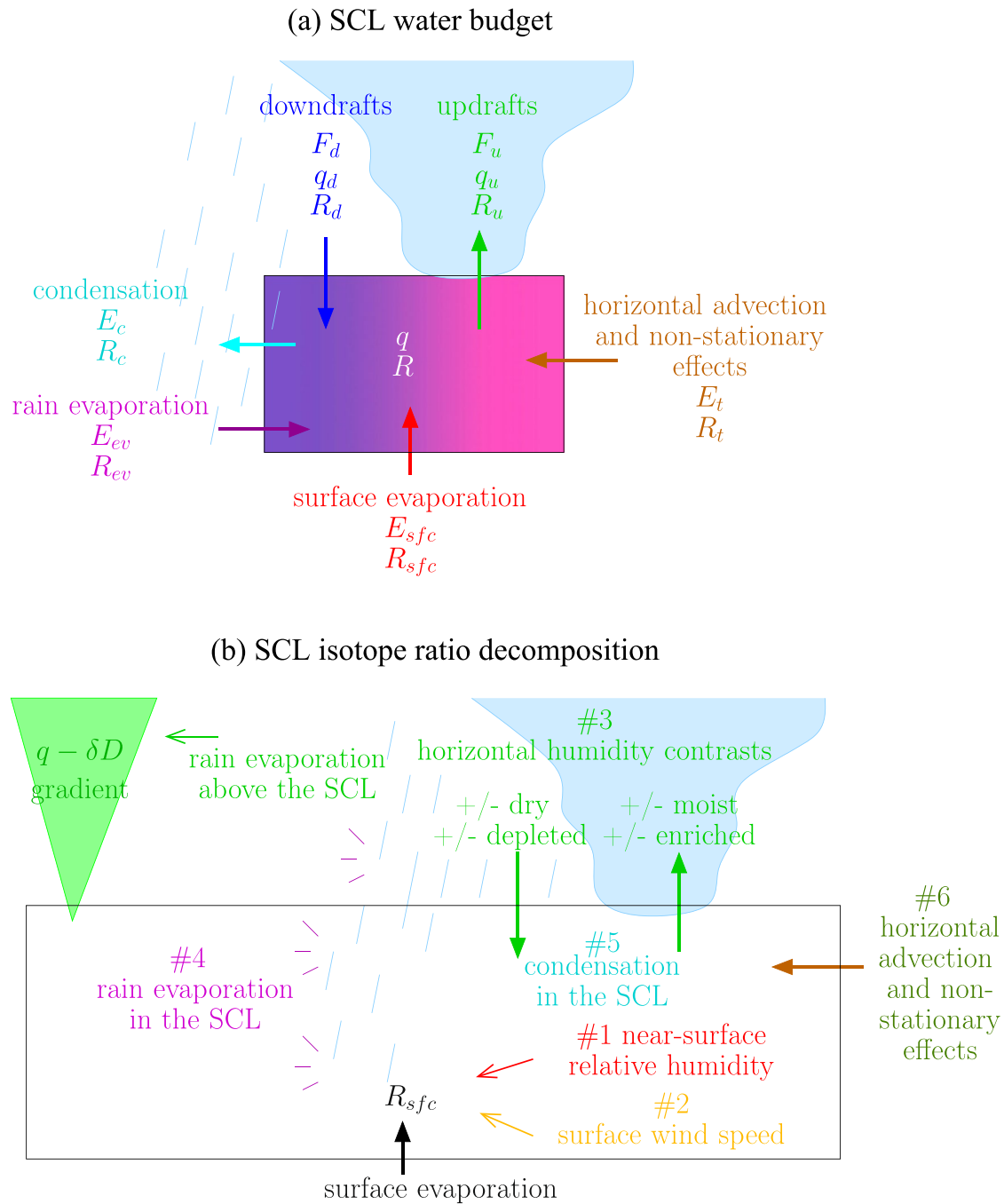


Figure 2. A description of the simple box model and of the decomposition of the sub-cloud layer (SCL) water vapor isotopic ratio into different contributions. (a) Simple model to predict the SCL water vapor composition. It accounts for surface evaporation, rain evaporation, cloud condensation, updrafts, and downdrafts at the SCL top, and horizontal advection and non-stationary effects quantified as a water budget residual. (b) The 6 contributions in the decomposition of the isotopic ratio: near-surface relative humidity (#1, red) and surface wind speed (#2, orange), which both contribute to control the isotope composition of the surface evaporation; horizontal humidity contrasts, and rain evaporation above the SCL (#3, green), which both contribute to the SCL depletion by vertical mixing; rain evaporation (#4, purple); condensation (#5, cyan) within the SCL; and horizontal and non-stationary effects (#6, dark green).

where E_{sfc} is surface evaporation, F_d and F_u are the downward and upward mass fluxes at SCL top, E_{horiz} is the flux of water through horizontal advection, E_{ev} is the rain evaporation, E_c is some condensation that may occur if the SCL top is not horizontally uniform, $r_u = q_u/q$, $r_d = q_d/q$, q_u and q_d are the specific humidity in updrafts and downdrafts. All these variables are directly diagnosed from the simulations for each sub-domains as detailed in Risi et al. (2021).

2.3.2. Isotopic Budget

As for the water vapor budget, the budget for heavy water vapor isotopes in the SCL is:

$$\frac{d(R \cdot W)}{dt} = R_{sfc} \cdot E_{sfc} + F_d(R_d \cdot q_d - R \cdot q) - F_u(R_u \cdot q_u - R \cdot q) + R_{horiz} \cdot E_{horiz} + R_{ev} \cdot E_{ev} - R_c \cdot E_c \quad (3)$$

where R is the isotopic ratio of the near-surface vapor, R_u and R_d are the isotopic ratios in updrafts and downdrafts, R_{sfc} , R_{horiz} , R_{ev} and R_c are the isotopic compositions of the surface evaporation, horizontal advection, rain evaporation, and condensation fluxes.

We define:

$$E_{res} = E_{horiz} - \frac{dW}{dt} \quad (4)$$

E_{res} is the flux of water through both horizontal advection and non-stationary effects, and is calculated as a residual. For example, in the cyclone's eyewall where the air is very moist (the relative humidity is greater than 95%), we expect that horizontal advection will have a drying effect, that is, $E_{horiz} < 0$. In addition, since the cyclone wanders across the domain, the eyewall often arrives in dry parts of the domain, that is, $\frac{dW}{dt} > 0$. Therefore, both horizontal advection and non-stationary effects contribute to drying the eyewall, that is, $E_{res} < 0$.

Similarly, we define the isotopic ratio of the flux R_{res} :

$$R_{res} = \frac{R_{horiz} \cdot E_{horiz} - \frac{d(R \cdot W)}{dt}}{E_{horiz} - \frac{dW}{dt}} \quad (5)$$

To solve the isotopic budget equation for R , the isotopic ratios R_{sfc} , R_d , R_u , R_{res} , R_{ev} and R_c are all expressed as a function of R . The isotopic ratio of surface evaporation is given by Craig and Gordon (1965):

$$R_{sfc} = \frac{R_{oce}/\alpha_{eq}(SST) - h \cdot R}{\alpha_K \cdot (1 - h)} \quad (6)$$

where R_{oce} is the isotopic ratio at the ocean surface, $\alpha_{eq}(SST)$ is the equilibrium fractionation coefficient at the SST, α_K is kinetic fractionation coefficient (Merlivat & Jouzel, 1979) and h is the relative humidity normalized at the SST and accounting for ocean salinity calculated as follows:

$$h = q/q_{sat}^{surf}(SST) \quad (7)$$

where $q_{sat}^{surf}(SST) = 0.98 \cdot q_{sat}(SST)$ and q_{sat} is the humidity saturation as a function of temperature at the sea level pressure. Variables h and the kinetic fractionation as a function of surface wind speed are diagnosed from the CRM. We assume that $\delta D_{oce} = 0\text{‰}$.

The isotopic ratios in updrafts and downdrafts are assumed to follow logarithmic functions: $R_u = R \cdot (r_u)^{\alpha_u - 1}$ and $R_d = R \cdot (r_d)^{\alpha_d - 1}$ where R_u and R_d are isotopic ratios in updrafts and downdrafts, and α_u and α_d are the $q - \delta D_v$ steepness coefficients for updrafts and downdrafts (Risi et al., 2020). We set $R_{res} = \phi_{res} \cdot R$, $R_{ev} = \phi_{ev} \cdot R$, and $R_c = \phi_c \cdot R$. All parameters α_u , α_d , ϕ_{res} , ϕ_{ev} and ϕ_c can be diagnosed from the simulation for each sub-domain.

$$R = \frac{R_{oce}/\alpha_{eq}(SST)}{h + \alpha_K \cdot (1 - h) \cdot A} \quad (8)$$

where

$$A = \frac{((r_u)^{\alpha_u} - 1) + \frac{F_d}{F_u} \cdot (1 - (r_d)^{\alpha_d}) - \frac{E_{ev}}{qF_u} \cdot \phi_{ev} + \frac{E_c}{qF_u} \cdot \phi_c - \frac{E_{res}}{qF_u} \cdot \phi_{res}}{(r_u - 1) + \frac{F_d}{F_u} \cdot (1 - r_d) - \frac{E_{ev}}{qF_u} + \frac{E_c}{qF_u} - \frac{E_{res}}{qF_u}} \quad (9)$$

In absence of vertical mixing ($r_u = r_d = 1$), rain evaporation, condensation, horizontal advection, and non-stationary effects ($E_{ev} = E_c = E_{res} = 0$), then $A = 1$ and Equation 8 reduced to the classical closure (Merlivat & Jouzel, 1979) (hereafter MJ79 closure).

Note that the diagnostic of E_{res} and ϕ_{res} as residuals guarantees that the water and isotopic budgets of the SCL are closed. However, it does not guarantee that Equation 8 with input parameters diagnosed from the CRM simulations yields exactly the same isotopic ratios as those directly simulated by the CRM. This is because many simplifying assumptions underlie the simple model. In particular, we neglect spatial and temporal co-variations between all the different parameters within each sub-domain. In addition, we diagnose the parameters related to vertical mixing (q_u , q_d , α_u , α_d) assuming a simple upstream advection scheme (Godunov, 1959), whereas the advection scheme in the SAM model is more sophisticated (Smolarkiewicz & Grabowski, 1990). As will be illustrated in Sections 4.3 and 4.4, the simple box model of this study systematically overestimates the δD_v simulated by the CRM by a few ‰, and systematically underestimates d_v by a few ‰. While we keep in mind these mismatches, we will show that the simple box model is nevertheless able to simulate the isotopic variations between different sub-domains of the cyclone and the squall line, justifying its relevance.

2.3.3. Method to Decompose Anomalies in Isotopic Ratios

To decompose the anomaly in the isotopic ratio in each sub-domain relative to that in the environment, we categorize the parameters controlling R in our simple box model into six processes:

1. Parameter h : near-surface relative humidity, which impacts the kinetic processes during ocean surface evaporation (Merlivat & Jouzel, 1979) (Figure 2b, red).
2. Parameter α_K : kinetic fractionation coefficient, which depends on the surface wind speed (Merlivat & Jouzel, 1979) (Figure 2b, orange).
3. Parameters F_d/F_u , r_u , r_d , α_u , and α_d : vertical mixing through the SCL top (green in Figure 2b). This includes the effect of the horizontal humidity contrasts (r_u and r_d). When horizontal humidity contrasts between dry and moist zones of a sub-domain are larger, dry subsiding regions import drier air and more depleted water vapor into the SCL, while ascending regions export moister air and more enriched water vapor from the SCL. This has thus a depleting effect. This also includes the effect of variations in the steepness of the relationship between q and δD_v for updrafts and downdrafts (α_u and α_d). When the $q - \delta D_v$ steepness is larger, downdrafts import more depleted vapor into the SCL and updrafts export more enriched vapor out of the SCL (Risi et al., 2021). The $q - \delta D_v$ steepness depends on the enriching or depleting processes that occur above the SCL. Typically, the dominant effect is rain evaporation above the SCL, which depletes the water vapor, especially near the melting level (Risi et al., 2021). While the effects of horizontal humidity contrasts and $q - \delta D_v$ steepness were separated in (Risi et al., 2021), here we combine these two effects to reduce non-linear effects during the decomposition.
4. Parameters $E_{\text{ev}}/(qF_u)$ and ϕ_{ev} : rain evaporation in the SCL (purple in Figure 2b).
5. Parameters $E_c/(qF_u)$ and ϕ_c : condensation in the SCL (cyan in Figure 2b).
6. Parameters $E_{\text{res}}/(qF_u)$ and ϕ_{res} : horizontal advection and non-stationary effects (dark green in Figure 2b).

We can thus write the isotopic ratio predicted by the simple box model in each sub-domain s as

$R_s = R(p_{s,1}, p_{s,2}, p_{s,3}, p_{s,4}, p_{s,5}, p_{s,6}) = R((p_{s,i})_{i=1,6})$, where $p_{s,i}$ is the vector of parameters corresponding to the process i and the sub-domain s , and R is the function defined in Equation 8. The difference between the isotopic ratio in the sub-domain and that in the environment thus writes:

$$\Delta R_s = R((p_{s,i})_{i=1,6}) - R((p_{e,i})_{i=1,6}) \quad (10)$$

where $p_{e,i}$ is the vector of parameters corresponding to the process i and the environment. For each sub-domain s and each process j , we estimate the contribution of process j to ΔR_s as:

$$c_{s,j} = R\left(\left(\frac{p_{s,i} + p_{e,i}}{2}\right)_{i=1,6,i \neq j}, p_{s,j}\right) - R\left(\left(\frac{p_{s,i} + p_{e,i}}{2}\right)_{i=1,6,i \neq j}, p_{e,j}\right) \quad (11)$$

Because R is a non-linear function of its parameters, $\sum_{j=1}^6 c_{s,j}$ does not necessarily equal ΔR_s . We estimate the impact of non-linear effects as a residual:

$$c_{s,non\ linear} = \Delta R_s - \sum_{j=1}^6 c_{s,j} \quad (12)$$

3. Simulated Patterns and Qualitative Comparison With Observations

3.1. Tropical Cyclone

3.1.1. Mesoscale Structure

To visualize the mesoscale structure of the tropical cyclone, in Figure 3 we plot maps of the precipitation rate, near-surface air temperature, surface pressure anomaly, near-surface relative humidity, near-surface water vapor δD and surface rain δD for an arbitrary snapshot. The simulated cyclone exhibits features that are typical of observed cyclones (Houze, 2010). It exhibits a small eye with weak precipitation (Figure 3a) and warm air (Figure 3b), consistent with the subsidence in the eye. The eye is surrounded by an eyewall and spiraling rain bands with intense precipitation and strong cyclonic winds. Around the cyclone, strong compensating subsidence develops, leading to a dry environment and some scattered, isolated cumulus and cumulonimbus clouds and their cold pools (Figures 3a, 3b, and 3d).

To better document the different parts of the tropical cyclone, we plot composites of meteorological and isotopic variables as a function of the distance r to the storm center (Figures 4 and 5). All 10 snapshots were used to compute the composites. The storm center is defined as the minimum surface pressure over the domain for each snapshot. The typical structure of a tropical cyclone is well captured:

- The eye is associated with minimum pressure (around 50 hPa lower than in the environment, typical of category 4 cyclones), a local minimum in precipitation, maximum near-surface air temperature, and relative humidity and weak winds (Figures 4a–4c). The eye is, however, too small to see the expected subsidence in Figure 4.
- The eyewall is associated with maximum precipitation and horizontal winds. The air is strongly ascending, almost saturated throughout the full troposphere (Figure 5a), and condensation is intense except in the shallow SCL (Figure 5c).
- Rainbands beyond the eyewall are associated with significant but weaker precipitation and winds. In rain band clouds, the condensation rate is large (orange shades in Figure 5c). Below the rain band clouds, the air is dry (Figure 5a), allowing large rates of snow sublimation and rain evaporation (blue shades in Figure 5c).

3.1.2. Definition of Sub-Domains

Based on the previous description of mesoscale structure, we divide all grid points into five sub-domains. These sub-domains are defined automatically based on some arbitrary thresholds, to which results are not crucially sensitive. We define:

- the “eye” as grid points with $r \leq r_{\text{wall}}$, where r_{wall} is the first r value for which the precipitation exceeds 20 times the domain-average precipitation (yellow rectangles in Figure 4).
- the “eyewall” as grid points with $r_{\text{wall}} < r \leq r_{\text{band}}$, where r_{band} is the first r value greater than r_{wall} and with the precipitation lower than 20 times the domain-average precipitation (blue rectangles in Figure 4).
- the “environment” as grid points with $r > r_{\text{env}}$, where r_{env} is the first r value greater than r_{band} and with the precipitation lower than 0.8 times the domain-average precipitation (white in Figure 4).

The precipitation thresholds have been adjusted so as to match the simulated cyclone structure to that described in previous studies (Houze, 2010). In between the eyewall and the environment (pink rectangles in Figure 4), rain bands are not radially symmetric. Therefore, we define “rain bands” as grid points with $r_{\text{band}} < r \leq r_{\text{env}}$ and precipitation greater than 4 times the domain-average precipitation, and “in between rain bands” as the other points.

3.1.3. Simulated Isotopic Evolution

The water vapor is most enriched in the eye and in the dry environment (Figures 3e, 3f, and 4e), and most depleted in heavy isotopes in the eyewall and spiraling rain bands. The water vapor d-excess is lower in the eye, and higher in the eyewall and rain bands (Figures 4e and 4f). The water vapor is more depleted and has a higher d-excess within the rain bands than between the rain bands (Figures 4d and 4e, dashed black).

The precipitation δD (δD_p) varies in concert with the water vapor δD (δD_v) where the precipitation is highest (Figure 4e, dashed black). The precipitation is slightly more depleted than if in equilibrium with the vapor. This suggests that the rain originates from condensation at a higher altitude and undergoes little evaporative enrichment as it falls, consistent with the high relative humidity. In addition, the rain quickly falls to the ground, leaving less time for the rain to isotopically equilibrate with the vapor.

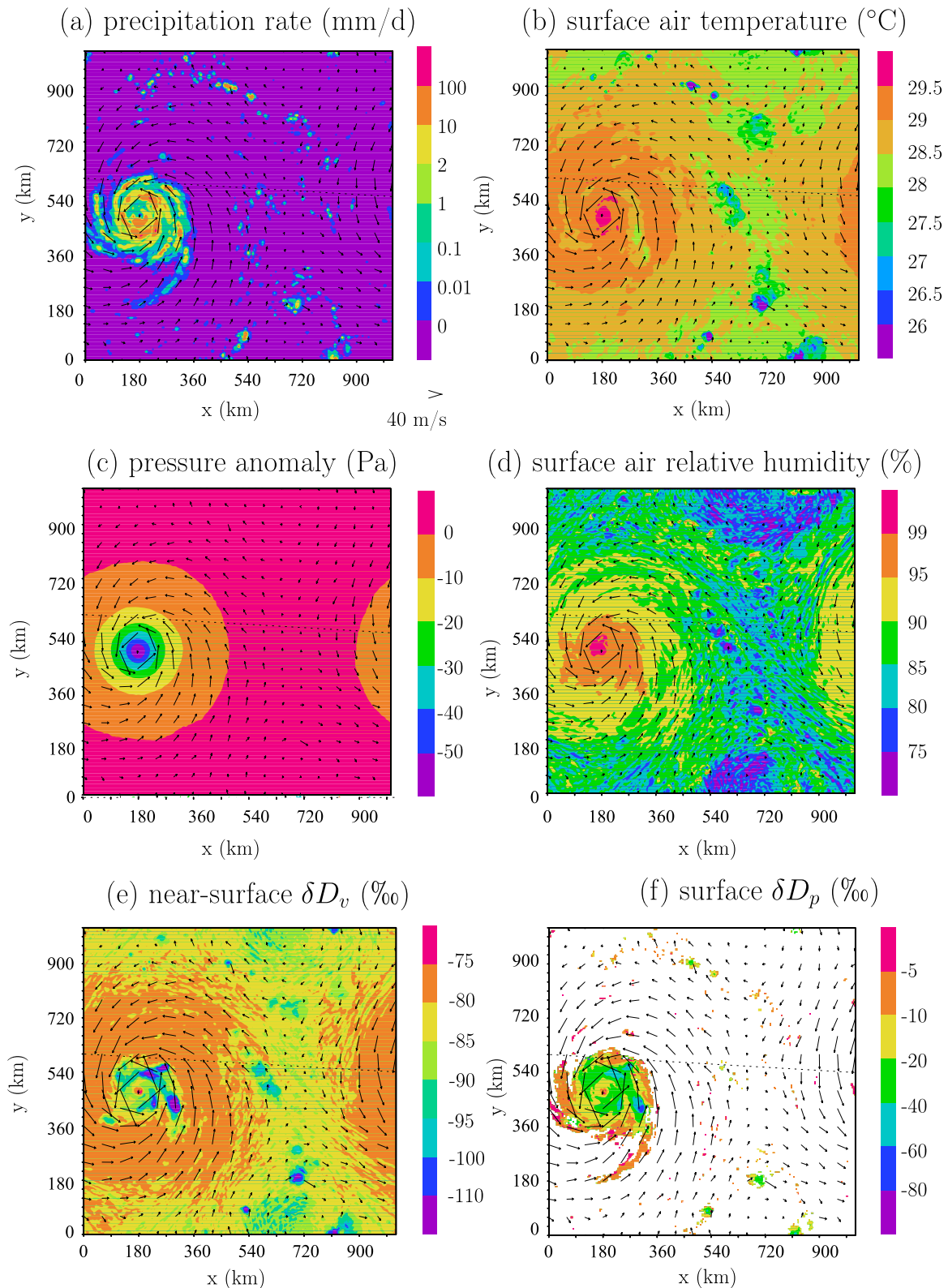


Figure 3. Snapshots of the cyclone simulation: (a) precipitation rate, (b) near-surface air temperature, (c) surface pressure anomaly relative to the domain-mean, (d) near-surface relative humidity, (e) near-surface δD_v , and (f) δD_p . The near surface winds are shown as arrows. Note that due to the doubly periodic domain, the missing part of the cyclone on the left edge of the domain appears on the right edge of the domain. The snapshot was chosen as the one where the cyclone is the closest to the center of the domain, for easier visualization.

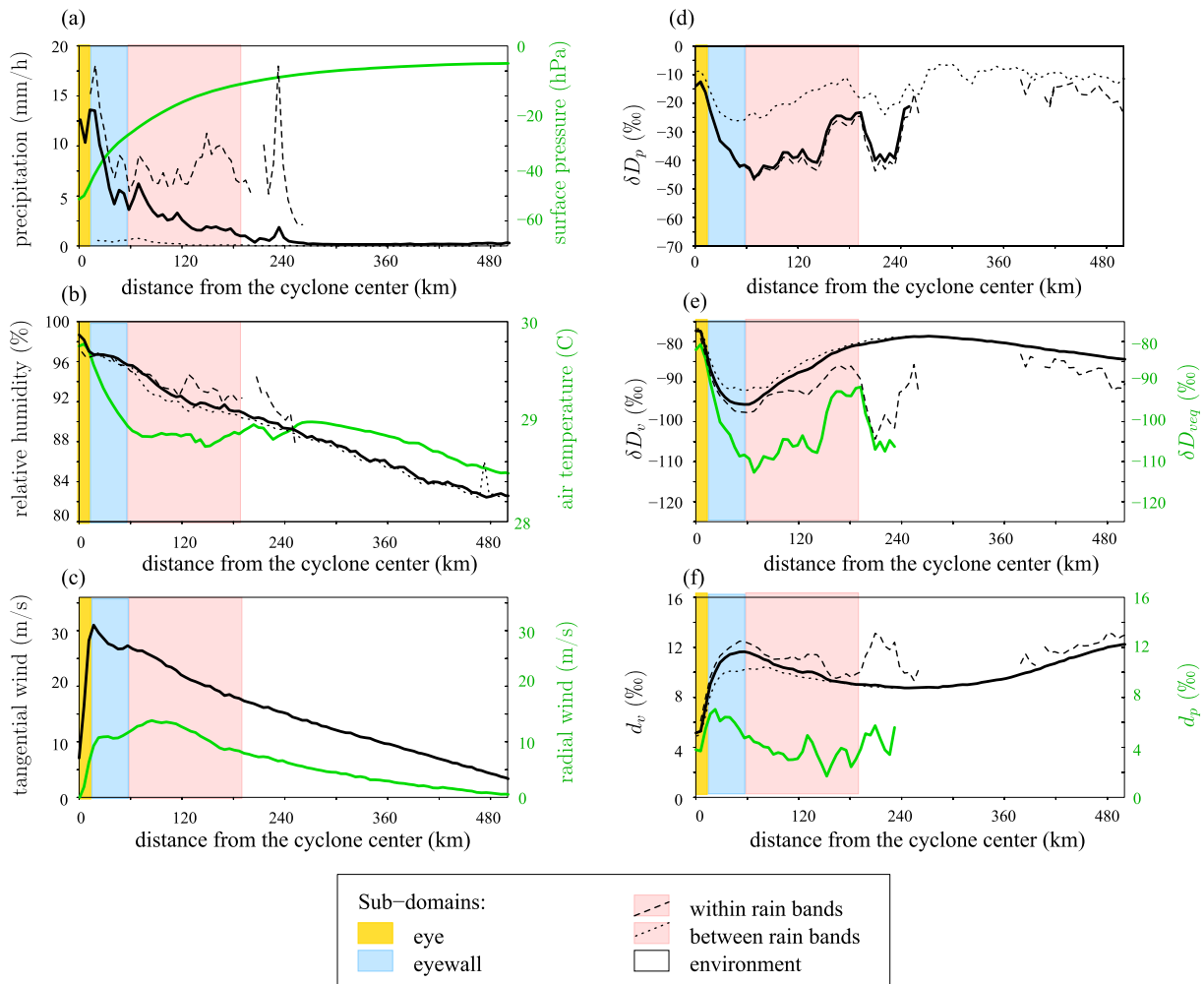


Figure 4. Evolution of surface variables as a function of distance to the cyclone center: precipitation rate (a, black), surface pressure (a, green), near-surface air temperature (b, black), near-surface relative humidity (b, green), tangential (c, black) and radial (c, green) wind, surface precipitation δD (d), near-surface water vapor δD (e, black), water vapor δD that would be in equilibrium with the precipitation (e, green), near-surface water vapor d-excess (f, black) and precipitation d-excess (f, green). The colored rectangles indicate the different sub-domains: the eye (yellow), the eyewall (blue), within and between rain bands (pink). The environment is in white. To distinguish between within rain bands and between rain bands, dashed and dotted black lines indicate the same as black lines but for grid points where the precipitation rate is respectively higher and lower than 4 times the domain-mean precipitation, representing respectively within rain bands and between rain bands.

3.1.4. Comparison With Isotopic Observations

Observed isotopic patterns in tropical cyclones can be diverse (Guilpart, 2018). However, some robust features emerge from the literature.

- There is a local maximum in δD_v and δD_p in the eye (Fudeyasu et al., 2008; Gedzelman et al., 2003). This is what the CRM simulates, with δD_v and δD_p slightly greater in the eye than in the environment (Figure 4e)
- Outside the eye, many studies have observed that the water vapor and precipitation are more depleted toward the storm center (Fudeyasu et al., 2008; Gedzelman et al., 2003; Jackisch et al., 2022; Munksgaard et al., 2015; Sanchez-Murillo et al., 2019; Skrzypek et al., 2019; Xu et al., 2019). This is what the CRM simulates (black line in the pink rectangle in Figure 4e).
- At a given distance from the storm center, the water vapor or precipitation is often more depleted within rain bands than in between (Guilpart, 2018; Munksgaard et al., 2015; Sun et al., 2022). This is also what the CRM simulates (Figure 4e, dashed black line relative to dotted black line).
- The observed d-excess in water vapor or precipitation is lower in the eye (Fudeyasu et al., 2008), higher in the environment and higher in the rain bands than in between (Munksgaard et al., 2015). These observations are consistent with our simulation (Figure 4f).

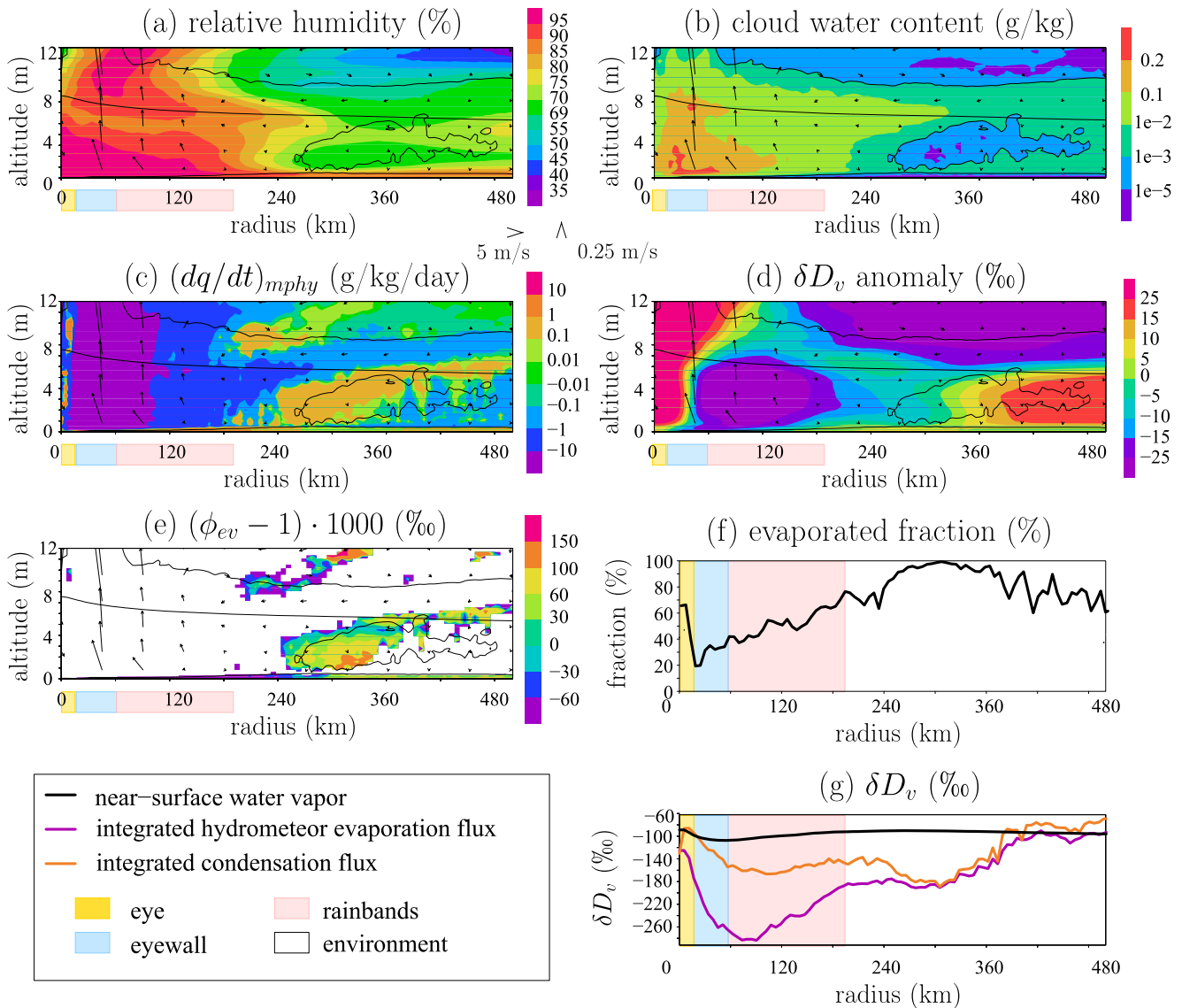


Figure 5. Variables as a function of altitude and of the distance r to the cyclone center: (a) Relative humidity; (b) cloud water content (cloud condensate and cloud ice); (c) specific humidity tendency due to phase changes (negative and positive values represent condensation/deposition and evaporation/sublimation respectively); (d) water vapor δD anomaly relative to the domain-mean δD_v at each level; (e) $(\phi_{ev} - 1) \cdot 1,000$, where $\phi_{ev} = R_{ev}/R_v$ is the relative enrichment of the isotopic ratio of the hydrometeor evaporation/sublimation relative to the water vapor isotopic ratio. ϕ_{ev} is shown only when significant hydrometeor evaporation/sublimation occurs; (f) fraction of the vertically integrated condensation flux that evaporates before reaching the ground; (g) δD in the near-surface vapor (black), in the vertically integrated condensation flux (orange) and in the vertically integrated evaporation flux (purple). The vertically integrated condensation and evaporation fluxes are calculated as the volumetric-mass weighted integrals of the specific humidity tendency due to phase changes (c) where the tendency is respectively negative and positive. In (a–e), the vectors show the radial and vertical components of the wind, with the vertical wind multiplied by 20 for better readability. The nearly horizontal black line shows the 0°C isotherm. The black contours highlight the 10^{-3} g/kg contour for cloud water content. The yellow, blue, and pink boxes indicate the eye, eyewall, and rainbands defined in Section 3.2.2.

3.2. Squall Line

3.2.1. Mesoscale Structure

In presence of wind shear, the convection organizes into lines of intense precipitation perpendicular to the imposed surface winds (Figure 6a). The environment is dry, with only a few isolated cumulonimbi. Under the squall line, a cold pool is driven by mesoscale downdrafts (Gamache & Houze, 1981; Zipser, 1977). The cold pool has a sharp edge at the front of the line, corresponding to the gust front, and a long trail due to the imposed rearward horizontal winds near the surface (Figure 6b).

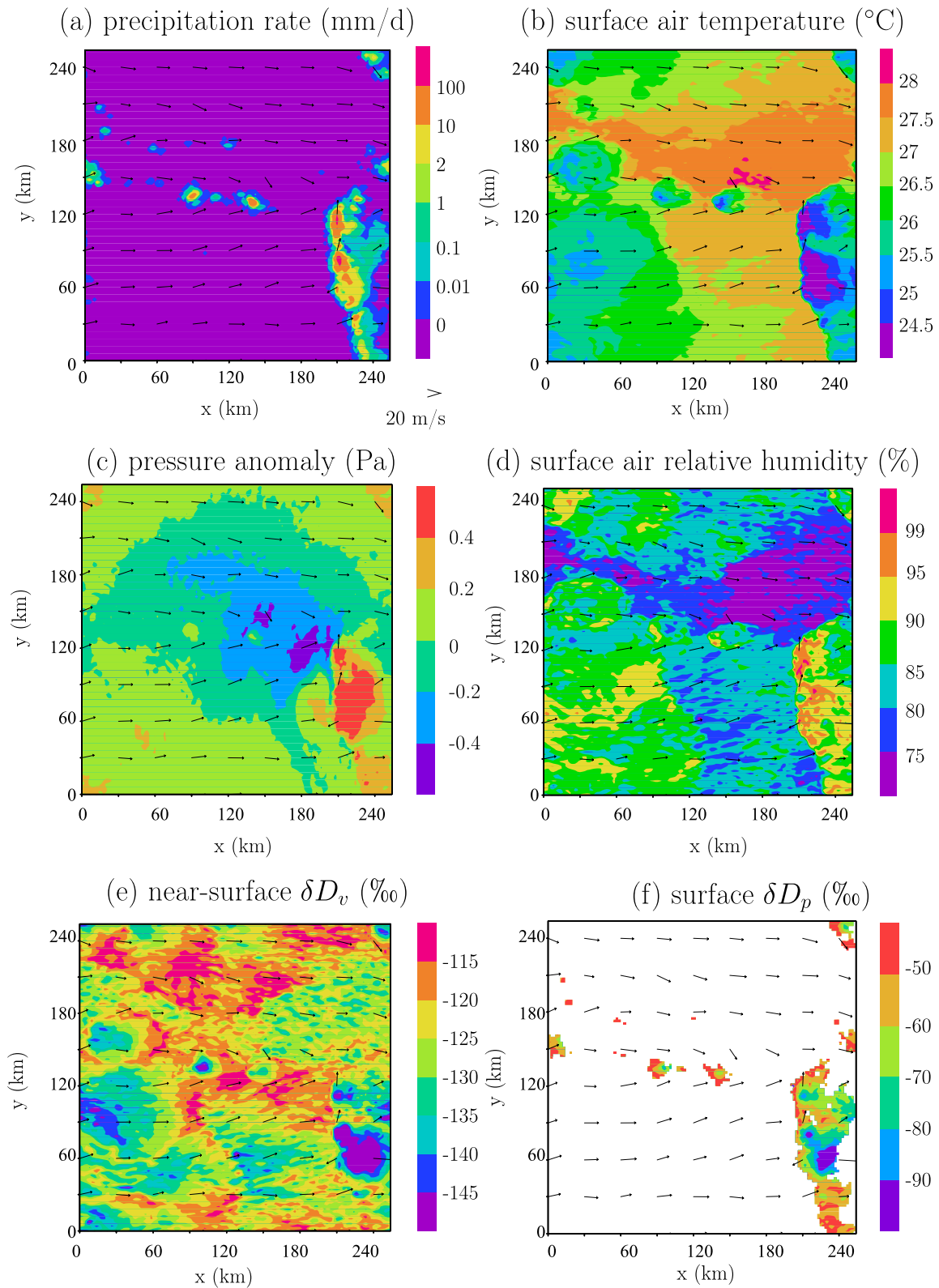


Figure 6. Same as Figure 3, except that a snapshot of the squall line simulation is shown. Note that due to the doubly periodic domain, the trailing region on the right edge of the domain continues on the left edge.

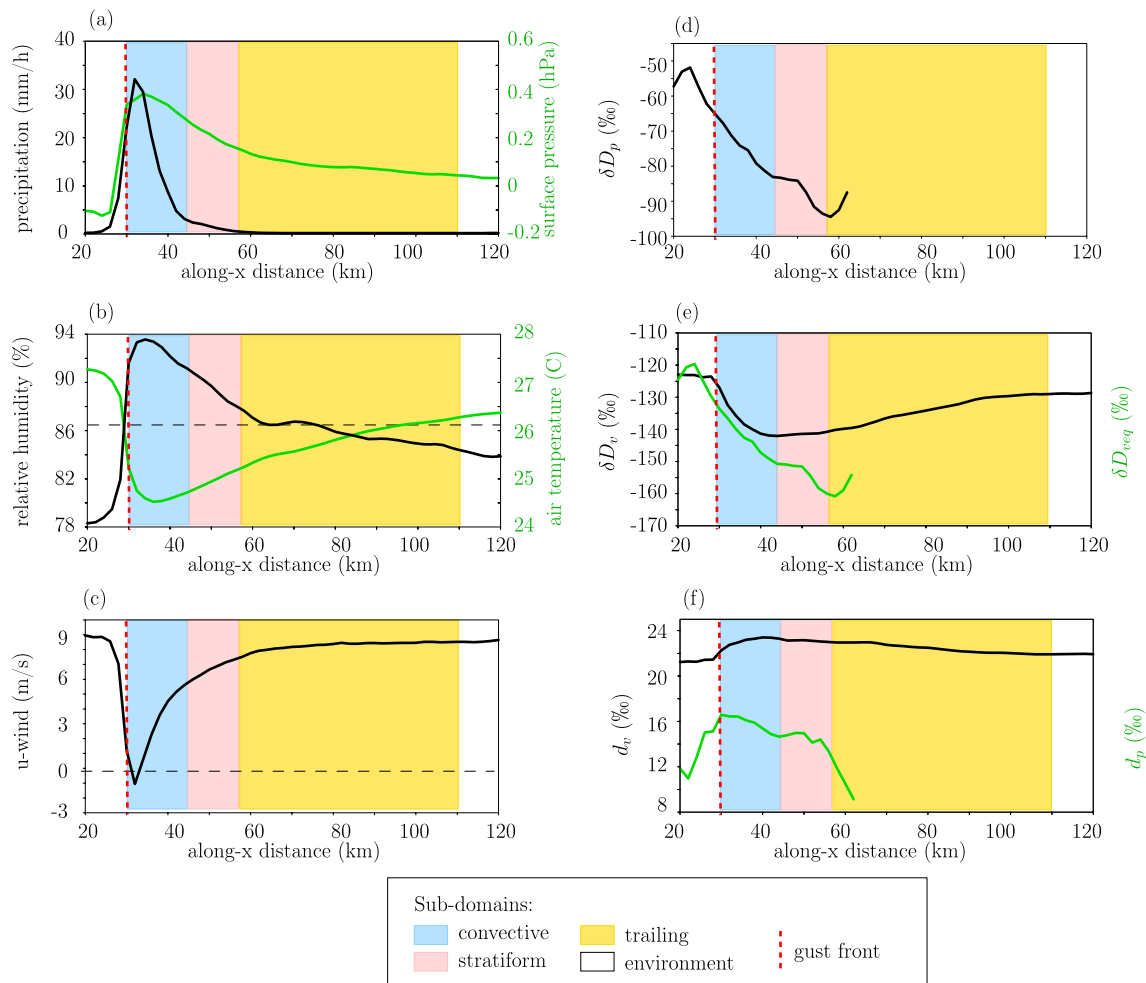


Figure 7. Same as Figure 4, except that variables for the squall line simulation are shown as a function of distance along the x -axis. The colored rectangles indicate the convective (blue), stratiform (pink), and trailing (yellow) sub-domains defined in Section 3.2.2. The location of the gust front is indicated by the vertical red dashed line.

To better document the different parts of the squall line, we plot composites of meteorological and isotopic variables as a function of the along- x distance to the gust front (Figures 7 and 8). For each snapshot and each value of y in the x - y domain, we select the value of x where the along- x gradient in surface pressure is at maximum. If the x -mean precipitation rate exceeds the x - y -mean value and if the gradient in surface pressure exceeds 1.7 Pa/km, we assume that it is a gust front. This procedure was visually defined to optimally detect gust fronts. We define a new x -axis and translate all rows so that all gust fronts of the different rows are aligned at $x_{gust} = 30$ km. We arbitrary set $x_{gust} = 30$ km so that the squall lines stand in the middle of the composite plots. Rows of the domain where the precipitation is lower than the domain mean, or where a gust front could not be identified, are considered “environment” and are not taken into account in the composite.

The precipitation rate is maximum just after the gust front (Figure 7a), consistent with observations (Chong, 2010). The precipitation maximum is located where the along- x near-surface surface wind becomes null (Figure 7c), favoring the maintenance of strong updrafts (Rotunno et al., 1988). Elsewhere, the surface wind blows rearward. Near the gust front, the temperature drops and the relative humidity rises (Figure 7b). The recovery to their environment value is slow due to the rearward advection.

Our simulated squall line shows only one precipitation peak. This is at odds with observations that often show two peaks, one for the convective region and one for the stratiform region, separated by a transition region (Biggerstaff & Houze, 1991; Chong, 2010). In our simulation, the convective region transitions continuously to the stratiform region. Increasing the horizontal resolution to 1 km did not help to simulate a transition region.

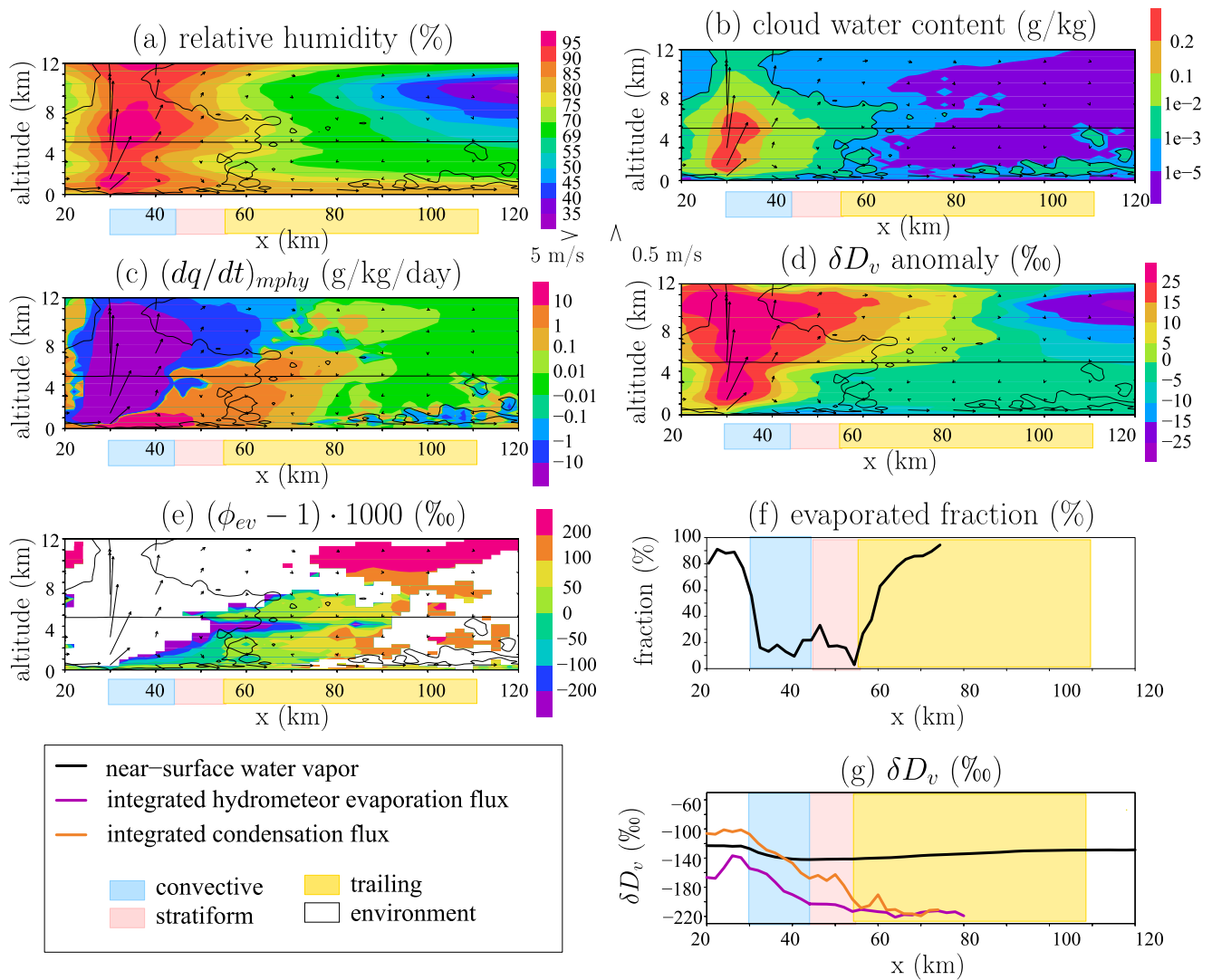


Figure 8. Same as Figure 5, except that variables for the squall line simulation are shown as a function of the distance along the x-axis. The blue, pink, and yellow boxes indicate the convective, stratiform, and trailing regions defined in Section 3.2.2.

In spite of this shortcoming, the convective and stratiform regions of the squall line can be identified from water vapor tendencies (Figure 8c). The convective region can be identified by its intense condensation throughout the entire troposphere (Figure 8c, around 50–60 km). The stratiform region can be identified by the condensation restricted to the upper troposphere (the anvil) and evaporation below (mesoscale downdraft) (Figure 8c, around 60–80 km). This pattern of condensation and evaporation is consistent with what we know from the squall line water budgets (Chong & Hauser, 1990; Gamache & Houze, 1983).

3.2.2. Definition of the Sub-Domains

Based on the above description of the mesoscale structure, we divide the grid points into four sub-domains: convective, stratiform, trailing, and environment, as detailed below. Given the continuous transition in our simulations, we define the convective and stratiform sub-domains based on a precipitation threshold. For rows where x_{gust} is defined, we define:

- the convective region with x between x_{gust} and x_{xconv} where x_{xconv} is the lowest x value greater than x_{gust} and where the precipitation is lower than eight times the domain-average precipitation (yellow rectangle in Figure 7). This precipitation threshold was adjusted to coincide with the transition from condensation through the entire troposphere to condensation above the melting level and rain evaporation below (Figure 8c), consistent with the transition from the convective to the stratiform region (Chong & Hauser, 1990; Gamache & Houze, 1983).

- the stratiform region with x between x_{conv} and x_{strati} , where x_{strati} is the lowest x value greater than x_{conv} and where the precipitation is below the domain-average precipitation (blue rectangle in Figure 7). This precipitation threshold was adjusted to coincide with the maximum extension of the anvil clouds, consistent with the typical structure of a squall line (Houze, 1977).

The horizontal winds near the surface spread the cold pool rearward beyond the precipitating region. Therefore, we also define a sub-domain called “trailing,” with x between x_{strati} and x_{trail} , where x_{trail} is the x value greater than x_{strati} and $T(x) < T(x_{\text{gust}}) - 1$, where T is the near-surface temperature in K (pink rectangle in Figure 7). All grid points that are not categorized as “convective,” “stratiform” or “trailing” are called “environment” (white in Figure 7).

3.2.3. Simulated Isotopic Evolution

Simulated squall lines show a progressive depletion of the vapor in the convective region, maximum depletion at the end of the convective region, and a long recovery in the stratiform and trailing regions (Figure 7e). The δD_v reaches its environment value about 100 km after the convective peak.

The δD_p varies in concert with δD_v (Figure 7d). In the convective and stratiform regions, δD_p is lower than in equilibrium with the vapor (green in Figure 7e), consistent with a quick fall and little evaporative enrichment. The weak precipitation that falls upwind of the convective region, where the air is dry, has a δD_p higher than that in equilibrium with vapor, indicating evaporative enrichment during rain evaporation.

The d-excess in the vapor is higher in the convective and stratiform regions, and to a lesser extent in the trailing region, than in the environment (Figure 7f). The low d-excess in the precipitation reflect the effect of evaporative enrichment, especially before the gust front and in the trailing region.

3.2.4. Comparison With Isotopic Observations

Isotopic observations during squall lines often show a “W” shape with minimum δD_p in the convective and stratiform regions and a local maximum in the transition region (Risi et al., 2010; Taupin & Gallaire, 1998). Our simulation is consistent with this observation, except that since our simulation does not exhibit any transition region, it shows a “V” shape instead of a “W” shape.

Investigation of the vapor isotopes of the squall lines in the Sahel showed that the isotopic evolution can be diverse, but some robust features emerge (Tremoy et al., 2014).

- In 80% of 74 observed squall lines (Tremoy et al., 2014), there is a depletion in the convective region compared to the environment before the squall line. This is consistent with our simulation.
- More than half of the observed squall lines show additional depletion in the stratiform region (Tremoy et al., 2014). This is also consistent with our simulation.
- For squall lines showing an isotopic depletion in the convective or stratiform region, the recovery from this depletion takes several hours after the end of the rain (Tremoy et al., 2014). Considering a propagation speed of about 20 m/s, this is consistent with the recovery distance of about 100 km in our simulation.
- In 78% of observed squall lines, the “W” shape often observed in the precipitation is not observed in the vapor (Tremoy et al., 2014). Our simulations are thus consistent with this majority of squall lines

Our simulated isotopic evolution during the squall line thus captures the features that are most commonly observed in squall lines. Some squall lines may feature different variations, and even enrichment in the convective and stratiform regions (Tremoy et al., 2014). To check whether our simulations could capture such a diversity of isotopic variations, we performed many sensitivity tests, including simulations without large-scale ascent, with large-scale ascent peaking in the upper troposphere to favor stratiform development (Su et al., 2000), increased horizontal resolution, interactive radiation, reduced sublimation or reduced rain evaporation to favor the maintenance of the stratiform region (Bryan & Morrison, 2012; Yang & Houze, 1995), bowling alley domain, or prescribed horizontal wind in the upper troposphere to favor the development of the stratiform region (Caniaux et al., 1994). Depending on the simulations, the stratiform region is more or less extended and the squall lines are more or less organized, but the meteorological and isotopic evolution is always similar. We thus keep in mind that our simulations match the majority of squall lines, but not all of them. In addition, some observed feature in squall lines over land, such as the enrichment of the water vapor in some stratiform regions due to nearly total evaporation of the rain in dry air (Tremoy et al., 2014), cannot be captured by our simulations with an oceanic setting that favors a relatively moist environment.

4. Understanding Mesoscale Isotopic Variations

Since δD in the precipitation varies in concert with δD in the SCL water vapor, we will focus most of this section on understanding mesoscale isotopic variations in the water vapor.

4.1. Impact of Rain Evaporation

Observational and modeling studies highlighted the key role of rain evaporation and rain-vapor exchanges in depleting the water vapor within organized systems (Lawrence et al., 2004; Tremoy et al., 2014; Xu et al., 2019). Around tropical cyclones and downwind of squall lines, dry air (Figures 5a and 8a) favors thick layer of rain evaporation in the middle and lower troposphere (orange shade in Figures 5c and 8c). Maximum evaporation occurs in the cold pool under the convective and stratiform regions of the squall line (red shade in Figure 8c). The fraction of the formed condensate that evaporates before reaching the ground is in the range of 0%–30% in the convective and stratiform regions of the squall line and 20%–40% in the eyewall of the cyclone. It increases to 40%–80% in the rain bands of the cyclone and reaches 100% in the trailing region of the squall line and in the environment of both systems (Figures 5f and 8f).

To analyze the isotopic effect of rain evaporation in more detail, we calculate $\phi_{ev} = R_{ev}/R_v$, where R_v and R_{ev} are the isotopic ratios in water vapor and in hydrometeor evaporation/sublimation. Hydrometeor evaporation/sublimation includes the evaporation of rain and cloud droplets (below the 0°C isotherm) and the sublimation of ice, snow or graupel (above the 0°C isotherm). ϕ_{ev} represents the isotope enrichment of hydrometeor evaporation relative to water vapor: if $(\phi_{ev} - 1) \cdot 1,000 > 0\%$, hydrometeor evaporation/sublimation enriches the water vapor; if $(\phi_{ev} - 1) \cdot 1,000 < 0\%$, hydrometeor evaporation/sublimation depletes the water vapor. R_{ev} is calculated as $(dq_{HDO}/dt)_{mphy}/(dq/dt)_{mphy}$, where q_{HDO} is the mixing ratio for HDO (i.e., the ratio of the mass of HDO molecules over the mass of dry air), q is the water vapor mixing ratio, and $(dq/dt)_{mphy}$ and $(dq_{HDO}/dt)_{mphy}$ are the water vapor and HDO tendencies associated with phase changes. If hydrometeor evaporation/sublimation occurs, then the $(dq/dt)_{mphy}$ tendency is positive. In contrast, if cloud condensation or deposition onto the snow, cloud ice or graupel occurs, then the $(dq/dt)_{mphy}$ tendency is negative. R_{ev} is calculated only where $(dq/dt)_{mphy} > 0$. We can see that near the rain bands of the cyclone and in the stratiform region of the squall line, there is a strongly depleting effect of rain evaporation just below the melting level (purple shade in Figures 5e and 8e, where the nearly horizontal black line indicates the 0°C isotherm). This is because just below the melting level, most of the rain originates from snow melt, which is more depleted than locally formed droplets because the snow has formed at higher altitudes (Risi et al., 2021). There is also a depleting effect in the SCL of the cyclone. The depleting effect of rain evaporation is associated with negative anomalies in water vapor δD in the rain bands and under the eyewall of the cyclone, and under the stratiform region of the squall line (purple shade in Figures 5d and 8d).

Figures 5g and 8g compare the δD in the near-surface vapor, the vertically integrated condensation flux and the vertically integrated hydrometeor evaporation flux. The δD in the vertically integrated condensation flux is most negative in the eyewall and rain bands of the cyclone and in the convective and stratiform regions of the squall line (orange in Figures 5f and 8f), consistent with the condensation occurring higher in altitude in anvil clouds (Figures 5b, 5c, 8b, and 8c). Where the formed condensate evaporates totally, or nearly totally, as is the case in the environment, then the δD in the vertically integrated hydrometeor evaporation flux equals that in the vertically integrated condensation flux (orange and purple lines are almost identical in Figures 5f and 8f). There, the rain evaporation has an enriching effect (yellow and orange shades in Figures 5e and 8e), consistent with Tremoy et al. (2014). In contrast, where the evaporated fraction is smaller and the air is moister, the δD in the vertically integrated hydrometeor evaporation flux is more depleted than in the vertically integrated condensation flux (orange in Figures 5f and 8f). This contributes to the depleting effect of the rain evaporation in the eyewall and rain bands of the cyclone and in the convective and stratiform regions of the squall line (purple shade in Figures 5e and 8e), and thus to the depleted water vapor in these regions (purple shade in Figures 5d and 8d, black line in Figures 5f and 8f).

To summarize, rain evaporation and diffusive exchanges deplete the water vapor under the convective and stratiform regions of the cyclone and of the squall line. This depletion is due to the higher condensation altitude, the lower evaporated fraction of the rain and the moister air in which the evaporation occurs. The depleting effect of rain evaporation and diffusive exchanges in stratiform regions of convective systems has already been highlighted in previous studies (Aggarwal et al., 2016; Kurita, 2013), including in cyclones (Lawrence et al., 2004; Munksgaard et al., 2015).

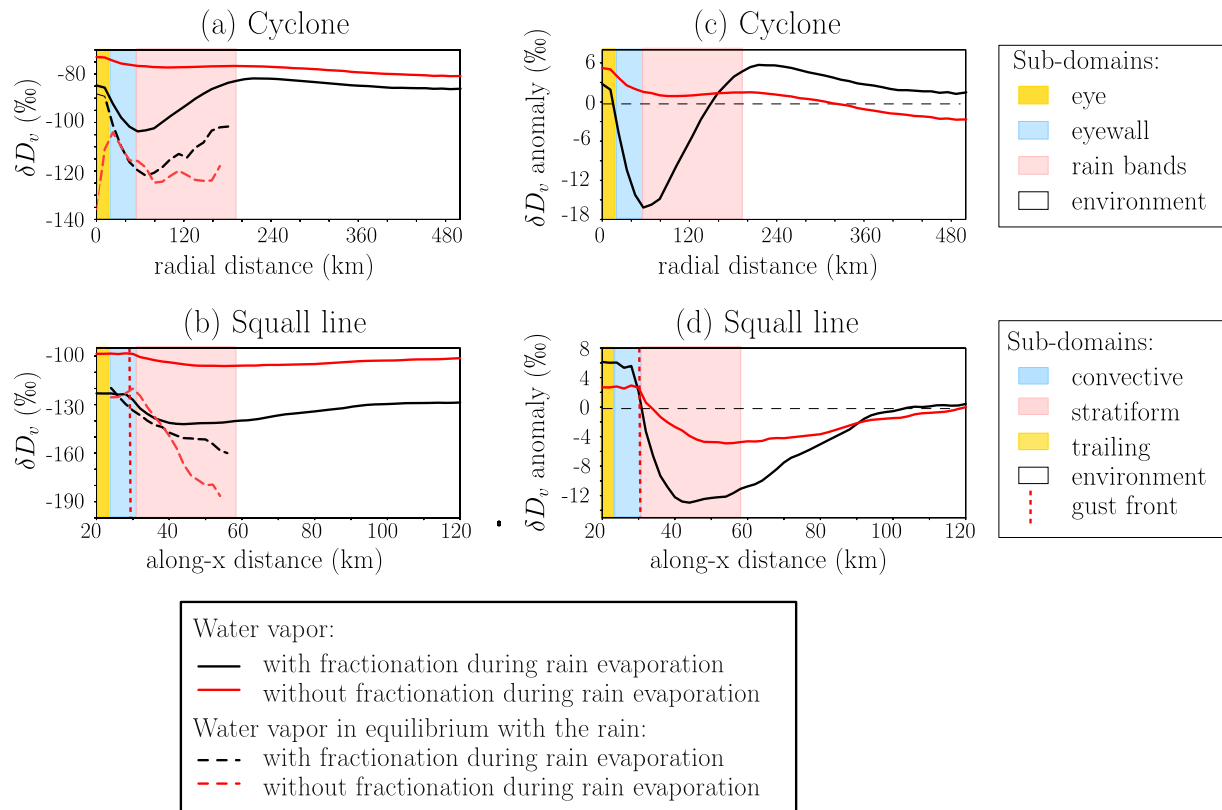


Figure 9. Results of the simulations with de-activated fractionation during rain evaporation. (a, b) Evolution of near-surface δD_v (solid) and of the water vapor δD in equilibrium with the near-surface precipitation (dashed) as a function of r for tropical cyclones (a) and as a function of x for squall lines (b), in simulations where rain evaporation and rain-vapor diffusive exchanges are activated (black) and de-activated (red). (c, d) Evolution of the near surface δD_v anomaly relative to the environment as a function of r for tropical cyclones (c) and as a function of x for squall lines (d).

4.2. Simulations With De-Activated Fractionation During Rain Evaporation

To quantify the effect of rain evaporation and rain-vapor diffusive exchanges, additional simulations in which these effects are de-activated were run, as in Field et al. (2010) and Risi et al. (2021). The fractionation coefficients were set to unity during all post-condensational processes. This impacts the simulation of isotopic variables, but not the simulation of meteorological variables.

Both in the cyclone and squall line simulations, δD_v would be higher without fractionation during rain evaporation than with fractionation (solid lines in Figures 9a and 9b), and the rain would be more depleted than if in equilibrium with the vapor (dashed lines in Figures 9a and 9b). The δD_p would be minimum under the rain bands in the cyclone simulation, and under the stratiform region in the squall line simulation, reflecting the higher condensation altitude in these regions (Section 4.1). With fractionation during rain evaporation, the rain-vapor diffusive exchanges make the vapor more isotopically enriched and the rain more isotopically depleted, thus bringing the rain and the vapor close to isotopic equilibrium (black lines in Figures 9a and 9b). This explains why δD_v and δD_p vary in concert. The δD_v is most negative where the condensation forms high in altitude and where the rain rate is strong enough to isotopically impact the water vapor. This explains why the δD_v is most negative near the transition between the eyewall and rainbands for the cyclone, and between the convective and stratiform region for the squall line (black solid lines in Figures 9a and 9b).

Without fractionation during rain evaporation, the mesoscale δD_v variations would be strongly reduced (Figures 9c and 9d). Peak-to-peak variations are respectively about 22‰ and 8‰ with and without fractionation in the cyclone case, and respectively 18‰ and 8‰ in the squall line case. This confirms the key role of rain evaporation and rain-vapor diffusive exchanges to deplete the low-level water vapor at the mesoscale scale.

4.3. Insights of the Simple Box Model for the Tropical Cyclone

To quantify the relative importance of different processes in different regions of the domain in the case of the cyclone, a simple box model of the SCL was designed (Section 2.3). We quantify the different terms of the water vapor budget in the different regions (Section 4.3.1), before evaluating the predictions by the simple box model and decomposing the isotopic differences for water vapor δD (Section 4.3.2) and d-excess (Section 4.3.3).

4.3.1. SCL Water Vapor Budget

The cyclone in itself (sub-domains eye, eyewall, rain bands, and between rain bands) covers less than 10% of the domain (Figure 10a). In all sub-domains, the main source of water vapor is surface evaporation (red in Figure 10b). Surface evaporation is more than twice larger in the eyewall, in rain bands and in-between rain bands than in the environment, consistent with the maximum winds. Surface evaporation is half smaller in the eye than in the environment, due to weak winds and moist near-surface air. Rain evaporation is also a significant moistening term in the eyewall and the rain bands (purple in Figure 10b). Condensation is insignificant (cyan in Figure 10b). Everywhere except in the eye, updrafts and downdrafts have a drying effect on the SCL (green and blue), because updrafts are preferentially moister and downdrafts are preferentially drier. In the eye, updrafts and downdrafts slightly moisten the SCL because the core of the eye is descending and almost saturated whereas air parcels near the eyewall may be drier and ascending. Horizontal advection and non-stationary effects dry the cyclone and slightly moisten the environment (dark green in Figure 10b). This is because dry air from the environment converge toward to cyclone center (horizontal advection effect). In addition, the cyclone wanders across the domain and thus mixes with air that was previously in the dry portions of the domain (non-stationary effect). In turn, in the wake of the cyclone, the environment is left moistened.

4.3.2. Evaluating and Decomposing the Water Vapor δD_v in Each Sub-Domain

In spite of its overestimate of the δD_v simulated by the CRM (green compared to red in Figure 11c), the simple box model is able to simulate the more depleted water vapor in all sub-domains relative to the δD_v simulated by the MJ79 closure (blue in Figure 10c) and to capture the main δD_v differences between the sub-domains: the slightly more enriched vapor in the eye relative to environment, the more depleted vapor in the eyewall, rain bands and between bands relative to the environment, and the more depleted vapor in the bands relative to in-between bands (Figure 10c).

The slightly more enriched vapor in the eye relative to the environment is mainly explained by the higher relative humidity (red in Figure 10d). When the relative humidity is close to 1, the vapor is nearly in equilibrium with the ocean. In this case, the influence of A in Equation 8 becomes small. As a consequence, the prediction by the simple box model is close to that of the MJ79 closure in the eye (blue in Figure 10c). In addition, in the eye, the rain evaporation is weak because there is little rain, and the horizontal advection into the eye is weak because the winds are mainly tangential, further limiting the influence of A in Equation 8. We note that a relative enrichment inside the eye is simulated in spite of the neglect of sea spray in our simulations. This does not exclude the possibility for a role of sea spray in nature (Fudeyasu et al., 2008), but this role is not necessary to explain the enrichment in the eye.

Figure 10d shows the decomposition of the δD_v anomaly for the different sub-domains relative to the environment. The more depleted vapor in the eyewall relative to the environment is mainly due to the enhanced depletion by vertical mixing through the SCL top (green in Figure 10d). The steeper isotopic gradient above the SCL, driven by the stronger rain evaporation above the SCL (Section 4.1), likely contributes to this term. The rain evaporation in the SCL also contributes to the more depleted vapor in the eyewall (purple in Figure 10d).

The more depleted vapor in the rain bands relative to the environment (and relative to between rain bands) is mainly due to the enhanced depletion by rain evaporation within the SCL (purple in Figure 10d). Alone, rain evaporation in the SCL would deplete the vapor in the rain bands by nearly 50% relative to the environment. As in the eyewall, the enhanced depletion by vertical mixing through the SCL top also contributes to the depletion (green in Figure 10d).

The more depleted vapor between rain bands relative to the environment is mainly due to the horizontal advection and non-stationary effects (dark green in Figure 10d). Horizontal winds bring depleted water vapor from the rain bands (Figure 10d). Consistently, horizontal advection has an enriching effect in rain bands, where the isotopic gradients are reversed: horizontal winds bring enriched water vapor from in-between rain bands.

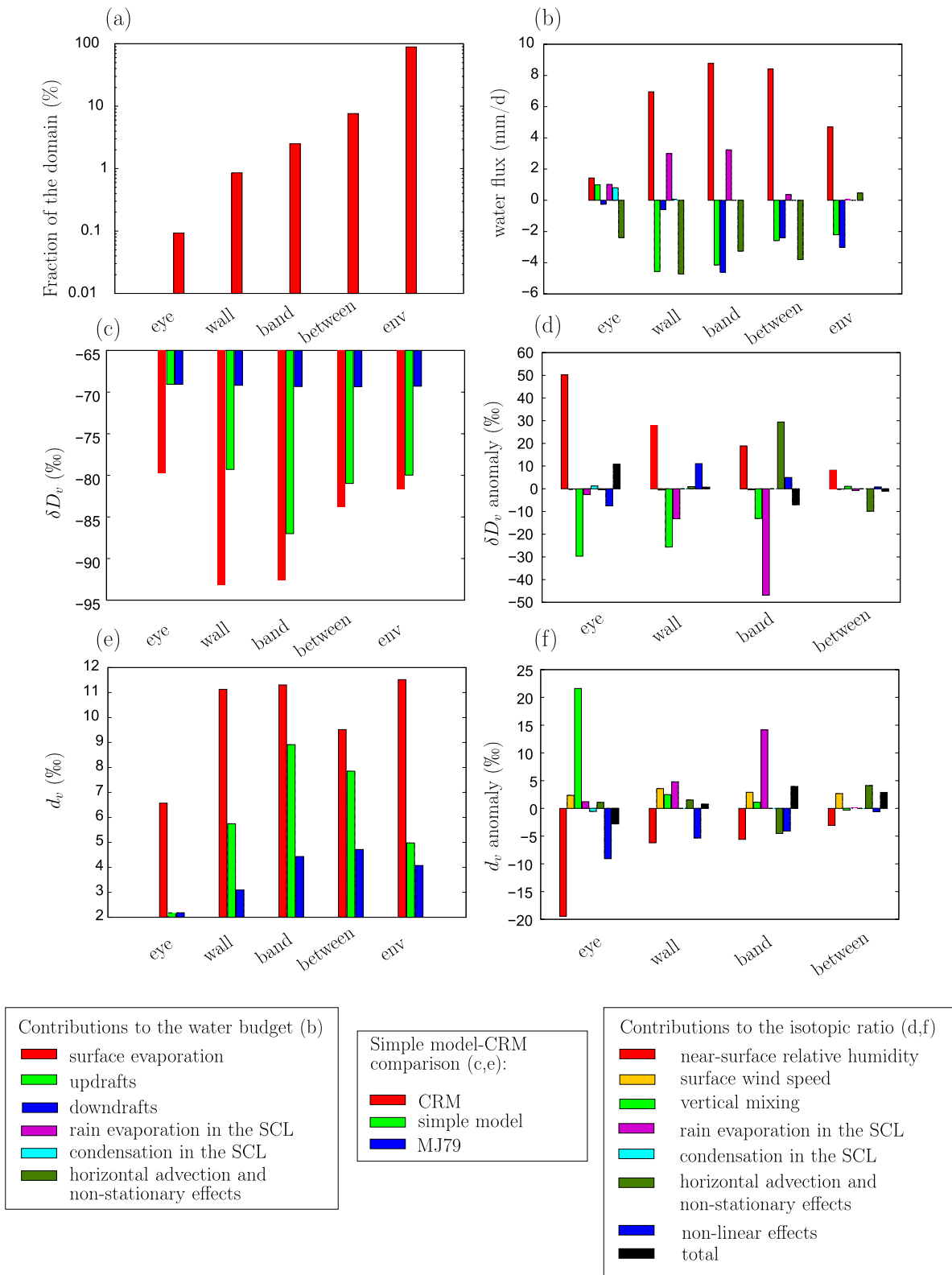


Figure 10.

The contributions of the kinetic fractionation during surface evaporation and of condensation in the SCL are marginal. The marginal impact of condensation is consistent with the absence of clouds in the SCL, and confirms that rain-out does not directly impact the SCL isotopic composition.

To summarize, the δD_v differences between the sub-domains are mainly explained by rain evaporation and rain-vapor diffusive exchanges inside the SCL, which deplete the eyewall and rain bands, consistent with previous studies (Gedzelman et al., 2003). Horizontal advection plays a key role to smooth the isotopic patterns, contributing to the progressive depletion as the air converges toward the center of cyclones suggested in previous studies (Gedzelman et al., 2003; Xu et al., 2019).

4.3.3. Evaluating and Decomposing the Water Vapor D-Excess in Each Sub-Domain

In spite of its underestimate of the d_v simulated by the CRM (green compared to red in Figure 10e), the model is able to capture the higher d_v than predicted by MJ79 closure (blue in Figure 10c) and several features simulated by the CRM: (a) the minimum d_v in the eye and (b) the higher d_v in the rain bands relative to between bands (Figure 10e). We will thus focus on understanding these two features:

1. The minimum d_v in the eye is due to the moist conditions that reduce the kinetic effects during surface evaporation (red in Figure 10f).
2. The higher d_v in the rain bands relative to the environment or between bands is mainly due to the rain evaporation in the SCL (purple in Figure 10f), which yields water vapor with high d-excess because of the relatively larger diffusivity of HDO relative to that of $H_2^{18}O$. Alone, it would contribute to an increase in d-excess by more than 15‰ relative to the environment.

As for δD_v , horizontal advection acts to smooth the d_v patterns, decreasing d_v in the rain bands and increasing it between rain bands (dark green in Figure 10f). The stronger the winds, the larger the kinetic fractionation during surface evaporation (yellow in Figure 10f). The contribution of this effect is however relatively small: alone, it would increase the d-excess by less than 5‰ in the eyewall, bands and in-between bands, relative to the environment (yellow in Figure 10f).

4.4. Insights of the Simple Box Model for the Squall Line

4.4.1. SCL Water Vapor Budget

The convective, stratiform and trailing regions of the squall line cover about 15% of the domain (Figure 11a). Surface evaporation is the main source of water in the SCL and is approximately uniform in all sub-domains (red in Figure 11b). The rain evaporation is a significant source in both the convective and stratiform parts (purple). In the convective part, the main sink of water is the export of moist air through updrafts (green in Figure 11b), consistent with the vigorous updrafts. Horizontal advection and non-stationary effects moisten the convective zone by advecting air from the stratiform region moistened by rain evaporation, and dries the trailing region by advecting drier air from the environment (dark green in Figure 11b).

4.4.2. Evaluating and Decomposing the Water Vapor δD_v in Each Sub-Domain

The box model performs better for the squall line than for the cyclone simulation. It captures well the relative variations across the sub-domains, in particular the maximum depletion in the stratiform region and the depletion in the convective and trailing regions relative to the environment (Figure 11c). We will thus focus on understanding these differences.

In both the convective and stratiform parts of the squall line, the depletion relative to the environment is mainly due to the rain evaporation and rain-vapor diffusive exchanges in the SCL that deplete the water vapor (purple

Figure 10. Results for the simple model of the sub-cloud layer (SCL) water vapor budget applied to the cyclone simulation. (a) Fraction of the domain, in log scale, covered by the five sub-domains of the cyclone: eye, eyewall (“wall”), rain bands (“bands”), in-between bands (“between”), and the environment (“env”). (b) Water fluxes contributing to the water budgets of the different sub-domains of the cyclone: Surface evaporation (red), updrafts (green), downdrafts (blue), rain evaporation (pink), condensation (cyan), and residual term associated with horizontal advection and non-stationary effects (dark green). (c) δD_v simulated by System for Atmospheric Modeling (red), by the simple model (green) and by the MJ79 closure (blue bars). (d) Decomposition of the δD_v anomaly in different sub-domains relative to the environment into 6 contributions: near-surface relative-humidity (red), surface wind speed (yellow), vertical mixing through the SCL top (green), rain evaporation within the SCL (purple), condensation within the SCL (cyan), and horizontal advection and non-stationary effects (dark green). The total is shown in black and non-linear effects are shown in blue. (e, f) Same as (c, d) but for d_v .

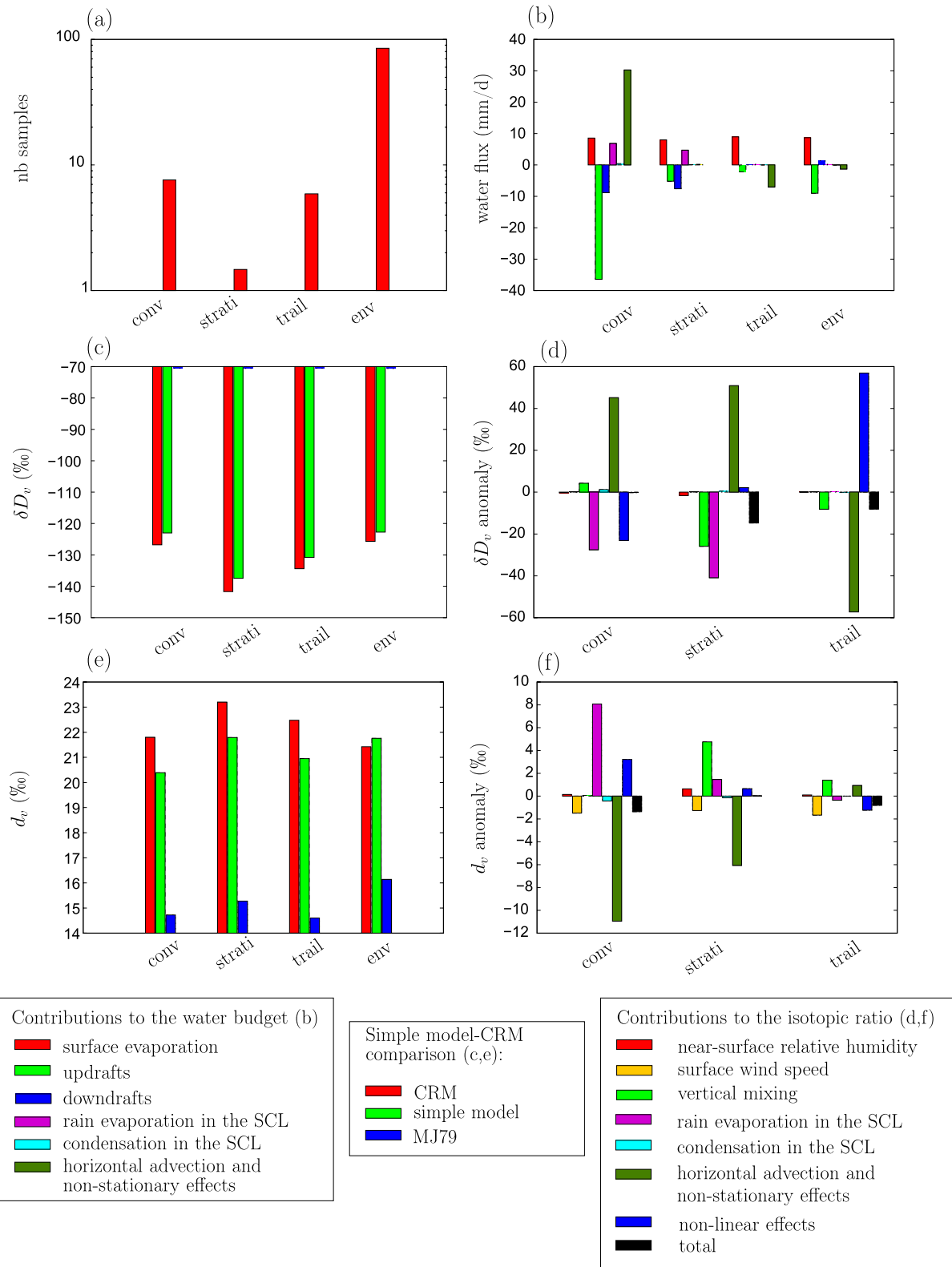


Figure 11. Results for the simple model of the sub-cloud layer (SCL) water vapor budget applied to the squall line simulation. Same as Figure 10 but for the four sub-domains of the squall line: convective (“conv”), stratiform (“strati”), and trailing (“trail”) regions, and the environment (“env”). Note that in panel (c), the prediction by the MJ79 closure (blue) is nearly -70% in all sub-domains, so it is hard to see.

in Figure 11d). Alone, it would deplete the convective and stratiform regions by about 30‰ and 45 ‰ respectively, far exceeding the total difference relative to the environment. In the stratiform region, vertical mixing, which likely includes the effect of rain evaporation above the SCL, also significantly contributes to the depletion (green in Figure 11d). This is consistent with the depleting effect of rain evaporation both in the SCL and near the melting level (Figure 8d), and with the major effect of fractionation during rain evaporation on the isotopic evolution in squall lines (Section 4.2).

In the trailing region, where the precipitation is weak, the depletion in heavy isotopes of the vapor is explained by horizontal advection and non-stationary effects (dark green in Figure 11d). Alone, it would contribute to a 55‰ depletion relative to the environment. This reflects the effect of horizontal advection spreading the depleted water vapor from the stratiform region. In contrast, the horizontal advection explains why the convective region is less depleted than the stratiform region: horizontal advection brings enriched water vapor from the environment toward the squall line front.

To summarize, the δD_v differences between the sub-domains are mainly explained by rain evaporation and rain-vapor diffusive exchanges inside the SCL, and also probably above the SCL. This is consistent with previous studies (Risi et al., 2010; Tremoy et al., 2014). Horizontal advection then plays a key role in spreading the isotopic anomaly rearward.

4.4.3. Evaluating and Decomposing the Water Vapor D-Excess in Each Sub-Domain

The simple box model is able to capture the fact that d_v is much larger than would be predicted by the MJ79 closure. It also captures the higher d_v in the stratiform region relative to the convective and trailing region.

The higher d_v in the stratiform region is mainly explained by the vertical mixing (green in Figure 11f). Vertical mixing probably brings water vapor with high d_v due to rain evaporation above the SCL. Rain evaporation in the SCL strongly increases d_v in the convective region (purple in Figure 11f), but this is compensated by the advection of vapor (dark green in Figure 11d). Since the environment has a lower d_v than the convective region (red in Figure 11c), the advection of air from the environment to the convective region acts to deplete the convective region. Variations in near-surface relative humidity and winds are smaller than in the cyclone simulations, so the contributions of these effects are marginal.

4.5. Discussion

We find many common aspects for the mesoscale isotopic variability between cyclone and squall line simulations.

- In both convective systems, rain evaporation, and rain-vapor diffusive exchanges both within and above the SCL (especially near the melting level) are the main drivers of the depletion in heavy isotopes of the vapor in the eyewall and rain bands for the cyclone, and in the convective and stratiform parts of the squall line. This is consistent with previous studies (Gedzelman et al., 2003; Tremoy et al., 2014; Xu et al., 2019). These processes have also a crucial impact on d-excess.
- In both cases, horizontal advection and non-stationary effects act to smooth the isotopic patterns. It leads to the gradual depletion toward the eyewall observed in tropical cyclones, and it spreads the isotopic anomalies rearward in the case of the squall line. This is consistent with previous studies (Xu et al., 2019).
- In both cases, the effect of condensation on the SCL water vapor is indirect. Condensation in the free troposphere maintains the vertical gradient in δD_v that allows the rain evaporation to have a depleting effect on the SCL water vapor. Through this indirect effect, condensation and precipitation are necessary for the depletion of the water vapor SCL (Yoshimura et al., 2003).

The main difference between the two convective systems is in the effect of kinetic effects during surface evaporation. Strong winds and moist conditions in tropical cyclones significantly impact the d-excess, whereas they have a marginal effect in squall lines.

Some similarities can also be found between processes controlling the isotopic composition in tropical cyclones and those in extra-tropical cyclones and cold fronts, as documented by previous studies (Aemisegger et al., 2015; Pfahl et al., 2012; Thurnherr & Aemisegger, 2022). Isotopically depleted water vapor and rain were observed in extratropical cyclones. This was explained by the interplay between air mass advection and depletion by rain-vapor interaction, consistent with our study, although in extratropical cyclones the large-scale advection

and large-scale gradients in temperature also contributed to depleting the vapor (Aemisegger et al., 2015; Pfahl et al., 2012). Low d_v was also observed in the warm sector of extratropical cyclones. As in tropical cyclones, this was explained by ocean evaporation in a moist environment, although in extratropical cyclones dew formation also contributes to lowering d_v (Thurnherr & Aemisegger, 2022).

5. Conclusion

Using CRM simulations of cyclones and squall lines, and a simple model for the SCL water vapor budget, we investigate how convective processes impact the isotopic composition of water vapor and precipitation at the mesoscale. We show that the main factors depleting heavy isotopes of the water vapor at the mesoscale is rain evaporation, especially in the SCL of rain bands and of the eyewall in tropical cyclones, and in the mesoscale downdraft of the stratiform region in squall lines (purple in Figure 12). The mesoscale δD_v patterns are subsequently reshaped by horizontal advection (orange in Figure 12). These mechanisms are overall consistent with those suggested in previous studies (Gedzelman et al., 2003; Tremoy et al., 2014; Xu et al., 2019). In contrast to these previous studies however, we highlight that condensation has no direct impact and that the evaporation of sea spray is not necessary to explain the relative enrichment in the cyclone eye.

This study contributes to our understanding of mesoscale isotopic variability. It provides physical arguments for the more depleted rain observed in tropical cyclones and squall lines relative to the rain in small-scale convection. Therefore, this study supports the interpretation of paleoclimate isotopic archives in tropical regions in terms of past cyclonic activity (Baldini et al., 2016; Medina-Elizalde & Rohling, 2012; Nott et al., 2007) or past frequency of large, long-lived, organized convective systems such as squall lines (Maupin et al., 2021).

However, when considering paleoclimate records at the annual scale or larger, the isotopic composition reflects an average over many convective systems of different organization types. In our simulations, this is equivalent to the domain-mean δD in simulations of tropical cyclones or squall lines relative to the domain-mean δD in simulations of isolated cumulonimbi, rather than the δD in tropical cyclone or squall lines relative to their environment in a given simulation. This paper focuses on mesoscale isotopic variations and does not discuss domain-mean values, because the realism of simulated mesoscale variations could be more easily assessed than the realism of domain-mean values. In particular, we realized that the domain-mean δD in the precipitation or water vapor of our tropical cyclone simulation was more enriched in heavy isotopes than that in simulations of squall lines or even of isolated cumulonimbi (Risi et al., 2020). This is at odds with observations of depleted cyclonic rains in the tropics (Lawrence et al., 2004). This discrepancy may be due to limitations in the radiative-convective equilibrium configuration. In radiative-convective equilibrium, the cyclone maintains a strong subsidence in its environment, which favors unrealistically dry conditions that allows enriched water vapor in the SCL to accumulate. In reality, tropical cyclones propagate and are thus not in equilibrium with their environment. In addition, tropical cyclones may occur in specific large-scale conditions. To account for the propagation of tropical cyclones and for the interplay with the large-scale circulation, more realistic simulations are necessary, for example, using regional cloud-resolving models (de Vries et al., 2022). In parallel, the interplay between large-scale circulation and convective organization deserves to be better documented in observations. It is possible that part of the observed depletion associated with tropical cyclones is mediated by large-scale conditions and domain-mean precipitation. To rigorously assess the role of convective organization, we would need to compare isotopic observations for different kinds of convective organization but for the same precipitation rate and large-scale context, as is now done for humidity (Tobin et al., 2012). This will allow us to rigorously assess the realism of the domain-mean isotopic composition in our simulations and will be the subject of a future study.

Finally, many other processes need to be investigated before drawing any paleoclimate conclusions from this study, including large-scale horizontal advection (Chen et al., 2021), land-atmosphere interactions along the air mass trajectories, infiltration processes, processes in the karstic systems and during calcite formation (Lases-Hernández et al., 2020). Our study is a first step toward a more comprehensive understanding of water isotopic variations.

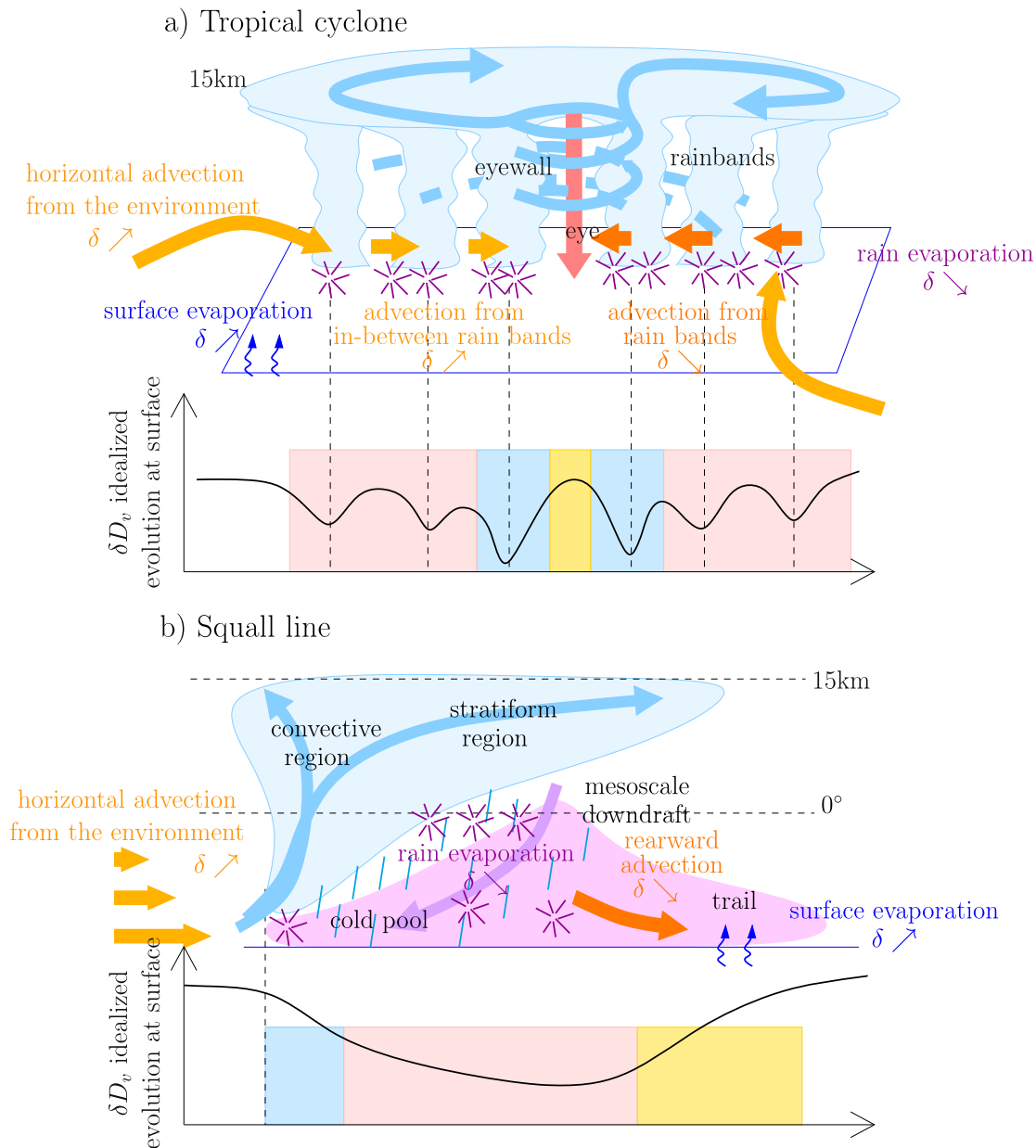


Figure 12. A schematic of the processes controlling the water vapor composition inside tropical cyclones (a) and squall lines (b). The key driver is rain evaporation, indicated by purple stars. Rain evaporation depletes water vapor in the rain bands and eyewall of tropical cyclones and in the convective and stratiform regions of squall lines. Horizontal advection then reshapes this pattern. Dark orange arrows indicate horizontal advection from depleted regions to less depleted regions, contributing to the spread of the depleted anomalies inward in cyclones and rearward in squall lines. Light orange arrows indicate horizontal advection from less depleted regions to more isotope depleted regions, partially compensating the depletion in most depleted regions.

Data Availability Statement

Information on SAM can be found on this web page: <http://rossby.msrc.sunysb.edu/~marat/SAM.html>. All simulation outputs used in this article are archived in the PANGAEA data repository: <https://doi.pangaea.de/10.1594/PANGAEA.937534>.

Acknowledgments

This work was granted access to the HPC resources of TGCC under the allocation 2092 and made by GENCI. CR, CM, and FV acknowledge the national french program INSU-LEFE for the funding of the SAM-iso proposal at the AO LEFE 2021. C.M. gratefully acknowledges funding from the European Research Council (ERC) under the European Union's Horizon 2020 research and innovation programme (Project CLUSTER, Grant 805041). P.B. was supported by the National Science Foundation under Grant AGS-1938108. G.V. contributed as part of his internship as a Master student at Sorbonne Université, with a funding from Paris Sciences & Lettres "ANR-10-IDEX-0001-02." C. D. contributed as part of her internship as a Bachelor student at Sorbonne Université. S.A. contributed as part of her PhD, with a funding from Ecole Normale Supérieure de Paris-Saclay. We thank all reviewers for their constructive comments.

References

- Abramian, S., Muller, C., & Risi, C. (2022). Shear-convection interactions and orientation of tropical squall lines. *Geophysical Research Letters*, 49(1), e2021GL095184. <https://doi.org/10.1029/2021GL095184>
- Aemisegger, F., Spiegel, J., Pfahl, S., Sodemann, H., Eugster, W., & Wernli, H. (2015). Isotope meteorology of cold front passages: A case study combining observations and modeling. *Geophysical Research Letters*, 42(13), 5652–5660. <https://doi.org/10.1002/2015gl063988>
- Aggarwal, P. K., Romatschke, U., Araguas-Araguas, L., Belachew, D., Longstaffe, F. J., Berg, P., et al. (2016). Proportions of convective and stratiform precipitation revealed in water isotope ratios. *Nature Geoscience*, 9(8), 624–629. <https://doi.org/10.1038/ngeo2739>
- Albright, A. L., Bony, S., Stevens, B., & Vogel, R. (2022). Observed subcloud layer moisture and heat budgets in the trades. *Journal of the Atmospheric Sciences*, 79(9), 2363–2385. <https://doi.org/10.1175/JAS-D-21-0337.1>
- Attinger, R., Spreitzer, E., Boettcher, M., Forbes, R., Wernli, H., & Joos, H. (2019). Quantifying the role of individual diabatic processes for the formation of PV anomalies in a North Pacific cyclone. *Quarterly Journal of the Royal Meteorological Society*, 145(723), 2454–2476. <https://doi.org/10.1002/qj.3573>
- Baldini, L. M., Baldini, J. U., McElwaine, J. N., Frappier, A. B., Asmerom, Y., Liu, K.-B., et al. (2016). Persistent northward North Atlantic tropical cyclone track migration over the past five centuries. *Scientific Reports*, 6(1), 37522. <https://doi.org/10.1038/srep37522>
- Bhattacharya, S. K., Sarkar, A., & Liang, M.-C. (2022). Vapor isotope probing of typhoons invading the Taiwan region in 2016. *Journal of Geophysical Research: Atmosphere*, 127(21), e2022JD036578. <https://doi.org/10.1029/2022JD036578>
- Biggerstaff, M. I., & Houze, R., Jr. (1991). Kinematic and precipitation structure of the 10–11 June 1985 squall line. *Monthly Weather Review*, 119(12), 3034–3065. <https://doi.org/10.1175/1520-0493>
- Blossey, P. N., Kuang, Z., & Romps, D. M. (2010). Isotopic composition of water in the tropical tropopause layer in cloud-resolving simulations of an idealized tropical circulation. *Journal of Geophysical Research*, 115(D24), D24309. <https://doi.org/10.1029/2010JD014554>
- Bony, S., Risi, C., & Vimeux, F. (2008). Influence of convective processes on the isotopic composition ($\delta^{18}\text{O}$ and δD) of precipitation and water vapor in the Tropics. Part I: Radiative-convective equilibrium and TOGA-COARE simulations. *Journal of Geophysical Research*, 113(D19), D19305. <https://doi.org/10.1029/2008JD009942>
- Bryan, G. H., & Morrison, H. (2012). Sensitivity of a simulated squall line to horizontal resolution and parameterization of microphysics. *Monthly Weather Review*, 140(1), 202–225. <https://doi.org/10.1175/MWR-D-11-00046.1>
- Caniaux, G., Redelsperger, J.-L., & Lafore, J.-P. (1994). A numerical study of the stratiform region of a fast moving squall line. Part I: General description and water and heat budgets. *Journal of the Atmospheric Sciences*, 51(14), 2046–2074. <https://doi.org/10.1175/1520-0469>
- Chakraborty, S., Sinha, N., Chattopadhyay, R., Sengupta, S., Mohan, P., & Datye, A. (2016). Atmospheric controls on the precipitation isotopes over the Andaman Islands, Bay of Bengal. *Scientific Reports*, 6(1), 1–11. <https://doi.org/10.1038/srep19555>
- Chavas, D. R., & Emanuel, K. (2014). Equilibrium tropical cyclone size in an idealized state of axisymmetric radiative-convective equilibrium. *Journal of the Atmospheric Sciences*, 71(5), 1663–1680. <https://doi.org/10.1175/JAS-D-13-0155.1>
- Chen, F., Huang, C., Lao, Q., Zhang, S., Chen, C., Zhou, X., et al. (2021). Typhoon control of precipitation dual isotopes in southern China and its palaeoenvironmental implications. *Journal of Geophysical Research: Atmospheres*, 126(14), e2020JD034336. <https://doi.org/10.1029/2020JD034336>
- Chong, M. (2010). The 11 August 2006 squall line system as observed from MIT Doppler radar during the AMMA SOP. *Quarterly Journal of the Royal Meteorological Society*, 136(S1), 209–226. <https://doi.org/10.1002/qj.466>
- Chong, M., & Hauser, D. (1990). A tropical squall line observed during the COPT81 experiment in west Africa: Part III: Heat and moisture budgets. *Monthly Weather Review*, 118(8), 1696–1706. <https://doi.org/10.1175/1520-0493>
- Conroy, J. L., Noone, D., Cobb, K. M., Moerman, J. W., & Konecky, B. L. (2016). Paired stable isotopologues in precipitation and vapor: A case study of the amount effect within western tropical Pacific storms. *Journal of Geophysical Research: Atmospheres*, 121(7), 3290–3303. <https://doi.org/10.1002/2015JD023844>
- Craig, H. (1961). Isotopic variations in meteoric waters. *Science*, 133(3465), 1702–1703. <https://doi.org/10.1126/science.133.3465.170>
- Craig, H., & Gordon, L. I. (1965). Deuterium and oxygen-18 variations in the ocean and marine atmosphere. In *Stable isotope in oceanographic studies and paleotemperatures* (pp. 9–130). Laboratorio di Geologia Nucleare.
- Cruz, F. W., Vuille, M., Burns, S. J., Wang, X., Cheng, H., Werner, M., et al. (2009). Orbitally driven east-west antiphasing of South American precipitation. *Nature Geoscience*, 2(3), 210–214. <https://doi.org/10.1038/ngeo444>
- Dansgaard, W. (1964). Stable isotopes in precipitation. *Tellus*, 16(4), 436–468. <https://doi.org/10.3402/tellusa.v16i4.8993>
- de Vries, A. J., Aemisegger, F., Pfahl, S., & Wernli, H. (2022). Stable water isotope signals in tropical ice clouds in the West African monsoon simulated with a regional convection-permitting model. *Atmospheric Chemistry and Physics*, 22(13), 8863–8895. <https://doi.org/10.5194/acp-22-8863-2022>
- Diekmann, C. J., Schneider, M., Knippertz, P., de Vries, A. J., Pfahl, S., Aemisegger, F., et al. (2021). A Lagrangian perspective on stable water isotopes during the West African monsoon. *Journal of Geophysical Research: Atmospheres*, 126(19), e2021JD034895. <https://doi.org/10.1029/2021jd034895>
- Dütsch, M., Pfahl, S., Meyer, M., & Wernli, H. (2018). Lagrangian process attribution of isotopic variations in near-surface water vapour in a 30-year regional climate simulation over Europe. *Atmospheric Chemistry and Physics*, 18(3), 1653–1669. <https://doi.org/10.5194/acp-18-1653-2018>
- Field, R. D., Jones, D. B. A., & Brown, D. P. (2010). The effects of post-condensation exchange on the isotopic composition of water in the atmosphere. *Journal of Geophysical Research*, 115, D24305. <https://doi.org/10.1029/2010JD014334>
- Field, R. D., Kim, D., LeGrande, A. N., Worden, J., Kelley, M., & Schmidt, G. A. (2014). Evaluating climate model performance in the tropics with retrievals of water isotopic composition from Aura TES. *Geophysical Research Letters*, 41(16), 6030–6036. <https://doi.org/10.1002/2014GL060572>
- Frappier, A. B., Sahagian, D., Carpenter, S. J., González, L. A., & Frappier, B. R. (2007). Stalagmite stable isotope record of recent tropical cyclone events. *Geology*, 35(2), 111–114. <https://doi.org/10.1130/G23145A.1>
- Fudeyasu, H., Ichiyangi, K., Sugimoto, A., Yoshimura, K., Ueta, A., Yamanaka, M. D., & Ozawa, K. (2008). Isotope ratios of precipitation and water vapor observed in Typhoon Shanshan. *Journal of Geophysical Research*, 113(D12), D12113. <https://doi.org/10.1029/2007JD009313>
- Gamache, J. F., & Houze, R. A. (1981). Mesoscale air motions associated with a tropical squall line. *Monthly Weather Review*, 110(2), 118–135. <https://doi.org/10.1175/1520-0493>
- Gamache, J. F., & Houze, R. A. (1983). Water budget of a mesoscale convective system in the tropics. *Journal of the Atmospheric Sciences*, 40(7), 1835–1850. [https://doi.org/10.1175/1520-0469\(1983\)040](https://doi.org/10.1175/1520-0469(1983)040)
- Gao, J., Masson-Delmotte, V., Risi, C., He, Y., & Yao, T. (2013). What controls southern Tibetan Plateau precipitation $\delta^{18}\text{O}$ at seasonal and intra-seasonal scales? A case study at Lhasa and Nyalam. *Tellus*, 65(1), 21043. <https://doi.org/10.3402/tellusb.v65i0.21043>

- Gedzelman, S., Lawrence, J., Gamache, J., Black, M., Hindman, E., Black, R., et al. (2003). Probing hurricanes with stable isotopes of rain and water vapor. *Monthly Weather Review*, 131(6), 112–1127. <https://doi.org/10.1175/1520-0493>
- Gentry, M. S., & Lackmann, G. M. (2010). Sensitivity of simulated tropical cyclone structure and intensity to horizontal resolution. *Monthly Weather Review*, 138(3), 688–704. <https://doi.org/10.1175/2009MWR2976.1>
- Godunov, S. K. (1959). Finite-difference methods for the numerical computations of equations of gas dynamics. *Math. Sb.*, 7, 271–290.
- Guilpart, E. (2018). Etude de la composition isotopique (deutérium et oxygène 18) de la vapeur d'eau dans l'atmosphère sur l'île de la réunion: Apport à la compréhension des processus humides atmosphériques en région tropicale. Unpublished doctoral dissertation.
- Houze, R. A. (1977). Structure and dynamics of a tropical squall line system. *Monthly Weather Review*, 105(12), 1540–1567. [https://doi.org/10.1175/1520-0493\(1977\)105<1540:sadoat>2.0.co;2](https://doi.org/10.1175/1520-0493(1977)105<1540:sadoat>2.0.co;2)
- Houze, R. A. (2004). Mesoscale convective systems. *Reviews of Geophysics*, 42(4), RG4003. <https://doi.org/10.1029/2004RG000150>
- Houze, R. A. (2010). Clouds in tropical cyclones. *Monthly Weather Review*, 138(2), 293–344. <https://doi.org/10.1175/2009MWR2989.1>
- Jackisch, D., Yeo, B. X., Switzer, A. D., He, S., Cantarero, D. L. M., Siringan, F. P., & Goodkin, N. F. (2022). Precipitation stable isotopic signatures of tropical cyclones in metropolitan manila, Philippines, show significant negative isotopic excursions. *Natural Hazards and Earth System Sciences*, 22(1), 213–226. <https://doi.org/10.5194/nhess-22-213-2022>
- Jakob, C., Singh, M., & Jungandreas, L. (2019). Radiative convective equilibrium and organized convection: An observational perspective. *Journal of Geophysical Research: Atmospheres*, 124(10), 5418–5430. <https://doi.org/10.1029/2018JD030092>
- Khairoutdinov, M., & Emanuel, K. (2013). Rotating radiative-convective equilibrium simulated by a cloud-resolving model. *Journal of Advances in Modeling Earth Systems*, 5(4), 816–825. <https://doi.org/10.1002/2013MS000253>
- Khairoutdinov, M., & Randall, D. A. (2003). Cloud resolving modeling of the ARM summer 1997 IOP: Model formulation, results, uncertainties, and sensitivities. *Journal of the Atmospheric Sciences*, 60(4), 607–625. <https://doi.org/10.1175/1520-0469>
- Kurita, N. (2013). Water isotopic variability in response to mesoscale convective system over the tropical ocean. *Journal of Geophysical Research: Atmospheres*, 118(18), 10–376. <https://doi.org/10.1002/jgrd.50754>
- Lacour, J.-L., Risi, C., Worden, J., Clerbaux, C., & Coheur, P.-F. (2017). Isotopic signature of convection's depth in water vapor as seen from IASI and TES D observations. *Earth and Planetary Science Letters*, 7(15), 9645–9663. <https://doi.org/10.5194/acp-17-9645-2017>
- Lases-Hernández, F., Medina-Elizalde, M., & Frappier, A. B. (2020). Drip water $\delta^{18}\text{O}$ variability in the northeastern Yucatán Peninsula, Mexico: Implications for tropical cyclone detection and rainfall reconstruction from speleothems. *Geochimica et Cosmochimica Acta*, 285, 237–256. <https://doi.org/10.1016/j.gca.2020.07.008>
- Lawrence, J. R. (1998). Isotopic spikes from tropical cyclones in surface waters: Opportunities in hydrology and paleoclimatology. *Chemical Geology*, 144(1–2), 153–160. [https://doi.org/10.1016/s0009-2541\(97\)00090-9](https://doi.org/10.1016/s0009-2541(97)00090-9)
- Lawrence, J. R., & Gedzelman, S. D. (1996). Low stable isotope ratios of tropical cyclone rains. *Geophysical Research Letters*, 23(5), 527–530. <https://doi.org/10.1029/96GL00425>
- Lawrence, J. R., & Gedzelman, S. D. (2003). Tropical ice core isotopes: Do they reflect changes in storm activity? *Geophysical Research Letters*, 30(2), 44–51. <https://doi.org/10.1029/2002GL015906>
- Lawrence, J. R., Gedzelman, S. D., Dexheimer, D., Cho, H.-K., Carrie, G. D., Gasparini, R., et al. (2004). Stable isotopic composition of water vapor in the tropics. *Journal of Geophysical Research*, 109(D6), D06115. <https://doi.org/10.1029/2003JD004046>
- Lawrence, J. R., Gedzelman, S. D., Gamache, J., & Black, M. (2002). Stable isotope ratios: Hurricane Olivia. *Journal of Atmospheric Chemistry*, 41(1), 67–82. <https://doi.org/10.1023/A:1013808530364>
- Lekshmy, P., Midhun, M., Ramesh, R., & Jani, R. (2014). ^{18}O depletion in monsoon rain relates to large scale organized convection rather than the amount of rainfall. *Scientific Reports*, 4(1), 5661. <https://doi.org/10.1038/srep05661>
- Maupin, C. R., Roark, E. B., Thirumalai, K., Shen, C.-C., Schumacher, C., Van Kampen-Lewis, S., et al. (2021). Abrupt Southern Great Plains thunderstorm shifts linked to glacial climate variability. *Nature Geoscience*, 14(6), 396–401. <https://doi.org/10.1038/s41561-021-00729-w>
- Medina-Elizalde, M., & Rohling, E. J. (2012). Collapse of Classic Maya civilization related to modest reduction in precipitation. *Science*, 335(6071), 956–959. <https://doi.org/10.1126/science.1216629>
- Merlivat, L., & Jouzel, J. (1979). Global climatic interpretation of the Deuterium-Oxygen 18 relationship for precipitation. *Journal of Geophysical Research*, 84(C8), 5029–5332. <https://doi.org/10.1029/JC084iC08p05029>
- Miller, D. L., Mora, C. I., Grissino-Mayer, H. D., Mock, C. J., Uhle, M. E., & Sharp, Z. (2006). Tree-ring isotope records of tropical cyclone activity. *Proceedings of the National Academy of Sciences of the United States of America*, 103(39), 14294–14297. <https://doi.org/10.1073/pnas.0606549103>
- Moerman, J. W., Cobb, K. M., Adkins, J. F., Sodemann, H., Clark, B., & Tuen, A. A. (2013). Diurnal to interannual rainfall $\delta^{18}\text{O}$ variations in northern Borneo driven by regional hydrology. *Earth and Planetary Science Letters*, 369, 108–119. <https://doi.org/10.1016/j.epsl.2013.03.014>
- Moore, M., Blossey, P., Muhlbauer, A., & Kuang, Z. (2016). Microphysical controls on the isotopic composition of wintertime orographic precipitation. *Journal of Geophysical Research: Atmospheres*, 121(12), 7235–7253. <https://doi.org/10.1002/2015JD023763>
- Moore, M., Kuang, Z., & Blossey, P. N. (2014). A moisture budget perspective of the amount effect. *Geophysical Research Letters*, 41(4), 1329–1335. <https://doi.org/10.1002/2013GL058302>
- Muller, C. (2013). Impact of convective organization on the response of tropical precipitation extremes to warming. *Journal of Climate*, 26(14), 5028–5043. <https://doi.org/10.1175/JCLI-D-12-00655.1>
- Muller, C., & Romps, D. M. (2018). Acceleration of tropical cyclogenesis by self-aggregation feedbacks. *Proceedings of the National Academy of Sciences of the United States of America*, 115(12), 2930–2935. <https://doi.org/10.1073/pnas.1719967115>
- Munksgaard, N. C., Zwart, C., Kurita, N., Bass, A., Nott, J., & Bird, M. I. (2015). Stable isotope anatomy of tropical cyclone Ita, north-eastern Australia, April 2014. *PLoS One*, 10(3), e0119728. <https://doi.org/10.1371/journal.pone.0119728>
- Neggens, R., Stevens, B., & Neelin, J. D. (2006). A simple equilibrium model for shallow-cumulus-topped mixed layers. *Theoretical and Computational Fluid Dynamics*, 20(5–6), 305–322. <https://doi.org/10.1007/s00162-006-0030-1>
- Nott, J., Haig, J., Neil, H., & Gillieson, D. (2007). Greater frequency variability of landfalling tropical cyclones at centennial compared to seasonal and decadal scales. *Earth and Planetary Science Letters*, 255(3–4), 367–372. <https://doi.org/10.1016/j.epsl.2006.12.023>
- Pfahl, S., Wernli, H., Yoshimura, K., & Dubey, M. (2012). The isotopic composition of precipitation from a winter storm—a case study with the limited-area model COSMO_{iso}. *Atmospheric Chemistry and Physics*, 12(3), 1629–1648. <https://doi.org/10.5194/acp-12-1629-2012>
- Price, R. M., Swart, P. K., & Willoughby, H. E. (2008). Seasonal and spatial variation in the stable isotopic composition ($\delta^{18}\text{O}$ and δD) of precipitation in south Florida. *Journal of Hydrology*, 358(3–4), 193–205. <https://doi.org/10.1016/j.jhydrol.2008.06.003>
- Ramos, R., LeGrande, A., Griffiths, M., Elsaesser, G., Litchmore, D., Tierney, J., et al. (2022). Constraining clouds and convective parameterizations in a climate model using paleoclimate data. *Journal of Advances in Modeling Earth Systems*, 14(8), e2021MS002893. <https://doi.org/10.1029/2021ms002893>

- Risi, C., Bony, S., Vimeux, F., Chong, M., & Descroix, L. (2010). Evolution of the water stable isotopic composition of the rain sampled along Sahelian squall lines. *Quarterly Journal of the Royal Meteorological Society*, *136*(S1), 227–242. <https://doi.org/10.1002/qj.485>
- Risi, C., Bony, S., Vimeux, F., Descroix, L., Ibrahim, B., Lebreton, E., et al. (2008). What controls the isotopic composition of the African monsoon precipitation? Insights from event-based precipitation collected during the 2006 AMMA campaign. *Geophysical Research Letters*, *35*(24), L24808. <https://doi.org/10.1029/2008GL035920>
- Risi, C., Muller, C., & Blosssey, P. (2020). What controls the water vapor isotopic composition near the surface of tropical oceans? Results from an analytical model constrained by large-eddy simulations. *Journal of Advances in Modeling Earth Systems*, *12*(8), e2020MS002106. <https://doi.org/10.1029/2020MS002106>
- Risi, C., Muller, C., & Blosssey, P. (2021). Rain evaporation, snow melt, and entrainment at the heart of water vapor isotopic variations in the tropical troposphere, according to large-eddy simulations and a two-column model. *Journal of Advances in Modeling Earth Systems*, *13*(4), e2020MS002381. <https://doi.org/10.1029/2020MS002381>
- Robe, F. R., & Emanuel, K. A. (2001). The effect of vertical wind shear on radiative–convective equilibrium states. *Journal of the Atmospheric Sciences*, *58*(11), 1427–1445. <https://doi.org/10.1175/1520-0469>
- Rotunno, R., Klemp, J. B., & Weisman, M. L. (1988). A theory for strong, long-lived squall lines. *Journal of the Atmospheric Sciences*, *45*(3), 463–485. <https://doi.org/10.1175/1520-0469>
- Sanchez-Murillo, R., Durán-Quesada, A. M., Esquivel-Hernández, G., Rojas-Cantillano, D., Birkel, C., Welsh, K., et al. (2019). Deciphering key processes controlling rainfall isotopic variability during extreme tropical cyclones. *Nature Communications*, *10*(1), 1–10. <https://doi.org/10.1038/s41467-019-12062-3>
- Sinha, N., & Chakraborty, S. (2020). Isotopic interaction and source moisture control on the isotopic composition of rainfall over the Bay of Bengal. *Atmospheric Research*, *235*, 104760. <https://doi.org/10.1016/j.atmosres.2019.104760>
- Skrzypek, G., Dogramaci, S., Page, G. F., Rouillard, A., & Grierson, P. F. (2019). Unique stable isotope signatures of large cyclonic events as a tracer of soil moisture dynamics in the semiarid subtropics. *Journal of Hydrology*, *578*, 124124. <https://doi.org/10.1016/j.jhydrol.2019.124124>
- Smolarkiewicz, P. K., & Grabowski, W. W. (1990). The multi-dimensional positive definite advection transport algorithm: Non-oscillatory option. *Journal of Computational Physics*, *86*(2), 355–375. [https://doi.org/10.1016/0021-9991\(90\)90105-A](https://doi.org/10.1016/0021-9991(90)90105-A)
- Stevens, B. (2006). Bulk boundary-layer concepts for simplified models of tropical dynamics. *Theoretical and Computational Fluid Dynamics*, *20*(5–6), 279–304. <https://doi.org/10.1007/s00162-006-0032-z>
- Su, H., Bretherton, C. S., & Chen, S. S. (2000). Self-aggregation and large-scale control of tropical deep convection: A modeling study. *Journal of the Atmospheric Sciences*, *57*(11), 1797–1816. <https://doi.org/10.1175/1520-0469>
- Sun, C., Tian, L., Shanahan, T. M., Partin, J. W., Gao, Y., Piatrunia, N., & Banner, J. (2022). Isotopic variability in tropical cyclone precipitation is controlled by Rayleigh distillation and cloud microphysics. *Communications Earth & Environment*, *3*(1), 1–10. <https://doi.org/10.1038/s43247-022-00381-1>
- Tan, J., Jakob, C., & Lane, T. P. (2013). On the identification of the large-scale properties of tropical convection using cloud regimes. *Journal of Climate*, *26*(17), 6618–6632. <https://doi.org/10.1175/JCLI-D-12-00624.1>
- Taupin, J.-D., & Gallaire, R. (1998). Variabilité isotopique à l'échelle infra-événement de quelques épisodes pluvieux dans la région de Niamey, Niger. *Comptes Rendus de l'Academie des Sciences - Series IIA: Earth and Planetary Science*, *326*(7), 493–498. [https://doi.org/10.1016/s1251-8050\(98\)80076-1](https://doi.org/10.1016/s1251-8050(98)80076-1)
- Thompson, G., Field, P. R., Rasmussen, R. M., & Hall, W. D. (2008). Explicit forecasts of winter precipitation using an improved bulk microphysics scheme. Part II: Implementation of a new snow parameterization. *Monthly Weather Review*, *136*(12), 5095–5115. <https://doi.org/10.1175/2008MWR2387.1>
- Thurnherr, I., & Aemisegger, F. (2022). Disentangling the impact of air-sea interaction and boundary layer cloud formation on stable water isotope signals in the warm sector of a southern ocean cyclone. *Atmospheric Chemistry and Physics*, *22*(15), 10353–10373. <https://doi.org/10.5194/acp-22-10353-2022>
- Tobin, I., Bony, S., & Roca, R. (2012). Observational evidence for relationships between the degree of aggregation of deep convection, water vapor, surface fluxes and radiation. *Journal of Climate*, *25*(20), 6885–6904. <https://doi.org/10.1175/JCLI-D-11-00258.1>
- Torri, G. (2021). On the isotopic composition of cold pools in radiative-convective equilibrium. *Journal of Geophysical Research: Atmosphere*, *126*(10), e2020JD033139. <https://doi.org/10.1029/2020jd033139>
- Torri, G. (2022). Isotopic equilibration in convective downdrafts. *Geophysical Research Letters*, *49*(15), e2022GL098743. <https://doi.org/10.1029/2022gl098743>
- Torri, G., Ma, D., & Kuang, Z. (2017). Stable water isotopes and large-scale vertical motions in the tropics. *Journal of Geophysical Research: Atmosphere*, *122*(7), 3703–3717. <https://doi.org/10.1002/2016JD026154>
- Tremoy, G., Vimeux, F., Mayaki, S., Souley, I., Cattani, O., Favreau, G., & Oi, M. (2012). A 1-year long delta¹⁸O record of water vapor in Niamey (Niger) reveals insightful atmospheric processes at different timescales. *Geophysical Research Letters*, *39*(8), L08805. <https://doi.org/10.1029/2012GL051298>
- Tremoy, G., Vimeux, F., Soumana, S., Souley, I., Risi, C., Cattani, O., & Oi, M. (2014). Clustering mesoscale convective systems with laser-based water vapor delta¹⁸O monitoring in Niamey (Niger). *Journal of Geophysical Research: Atmospheres*, *119*(9), 5079–5103. <https://doi.org/10.1002/2013JD020968>
- Vimeux, F., Gallaire, R., Bony, S., Hoffmann, G., & Chiang, J. C. H. (2005). What are the climate controls on deltaD in precipitation in the Zongo Valley (Bolivia)? Implications for the Illimani ice core interpretation. *Earth and Planetary Science Letters*, *240*(2), 205–220. <https://doi.org/10.1016/j.epsl.2005.09.031>
- Vimeux, F., Tremoy, G., Risi, C., & Gallaire, R. (2011). A strong control of the South American SeeSaw on the intraseasonal variability of the isotopic composition of precipitation in the Bolivian Andes. *Earth and Planetary Science Letters*, *307*(1–2), 47–58. <https://doi.org/10.1016/j.epsl.2011.04.031>
- Wang, Y. J., Cheng, H., Edwards, R. L., An, Z. S., Wu, J. Y., Shen, C. C., & Dorale, J. A. (2001). A high-resolution absolute-dated late Pleistocene Monsoon record from Hulu Cave, China. *Science*, *294*(5550), 2345–2348. <https://doi.org/10.1126/science.106461>
- Welsh, K., & Sánchez-Murillo, R. (2020). Rainfall, groundwater, and surface water isotope data from extreme tropical cyclones (2016–2019) within the Caribbean Sea and Atlantic Ocean basins. *Data in Brief*, *30*, 105633. <https://doi.org/10.1016/j.dib.2020.105633>
- Worden, J., Noone, D., & Bowman, K. (2007). Importance of rain evaporation and continental convection in the tropical water cycle. *Nature*, *445*(7127), 528–532. <https://doi.org/10.1038/nature05508>
- Xu, T., Sun, X., Hong, H., Wang, X., Cui, M., Lei, G., et al. (2019). Stable isotope ratios of typhoon rains in Fuzhou, Southeast China, during 2013–2017. *Journal of Hydrology*, *570*, 445–453. <https://doi.org/10.1016/j.jhydrol.2019.01.017>

- Yang, M.-H., & Houze, R. A., Jr. (1995). Sensitivity of squall-line rear inflow to ice microphysics and environmental humidity. *Monthly Weather Review*, *123*(11), 3175–3193. <https://doi.org/10.1175/1520-0493>
- Yoshimura, K., Oki, T., Ohte, N., & Kanae, S. (2003). A quantitative analysis of short-term O^{18} variability with a Rayleigh-type isotope circulation model. *Journal of Geophysical Research*, *108*(D20), 4647. <https://doi.org/10.1029/2003JD003477>
- Zipser, E. (1977). Mesoscale and convective scale downdrafts as distinct components of squall-line structure. *Monthly Weather Review*, *105*(12), 1568–1589. <https://doi.org/10.1175/1520-0493>